STANFORD UNIVERSITY

CENTER FOR SYSTEMS RESEARCH

Guidance for a Tilt-Rotor VTOL Aircraft During Takeoff and Landing

by

Narendra K. Gupta
and
Arthur E. Bryson, Jr.

Guidance and Control Laboratory

GUIDANCE FOR A TILT-ROTOR VTOL AIRCRAFT DURING TAKEOFF AND LANDING

by

Narendra K. Gupta
and
Arthur E. Bryson, Jr.

December 1972

SUDAAR No. 448

Prepared under

NAS-2-5143 for the U.S. Army
Air Research and Mobility Command,
Ames Directorate, NASA Ames Research
Center, Moffett Field, California

Department of Aeronautics and Astronautics
Stanford University
Stanford, California

ABSTRACT

A perturbation guidance scheme is developed to keep a tilt-rotor VTOL aircraft close to a predetermined nominal flight path during take-off and landing.

A simulation of the guidance scheme applied to the Bell Model 266 tilt-rotor VTOL gave satisfactory behavior in the presence of initial errors and wind disturbances.

CONTENTS

LIST OF ILLUSTRATIONS

LIST OF TABLES

CHAPTER I
Introduction

Vertical take-off and landing (VTOL) aircraft offer a potentially useful means of short-haul transportation. Since they do not require long runways for take-off and landing, it is possible to provide convenient air service using only small land areas for terminals.

Several different kinds of VTOL aircraft have been built and flown in the past decade. The tilting proprotor VTOL aircraft promises to be among the most efficient and least noisy during transition and hover. However, it has only a moderate cruise speed.

For economic viability, VTOL aircraft must be capable of operating (a) at night, (b) in fog, haze and cloudy weather, (c) near tall buildings, and (d) in a crowded air traffic environment. Because of the low departure and approach speeds of these aircraft there may be many aircraft in the vicinity of the airport during peak travel periods. Therefore, it is important to devise a good guidance scheme for these aircraft in the terminal area.

The present report describes a guidance scheme for a tilt-rotor aircraft during take-off and landing. The scheme has been simplified as much as possible to permit its implementation with an onboard computer. The Bell Model 266 is taken as the example aircraft.

Chapter II develops a mathematical model for the longitudinal motion of a tilting proprotor VTOL aircraft.

Chapter III describes the technique used for finding guidance laws during take-off and landing.

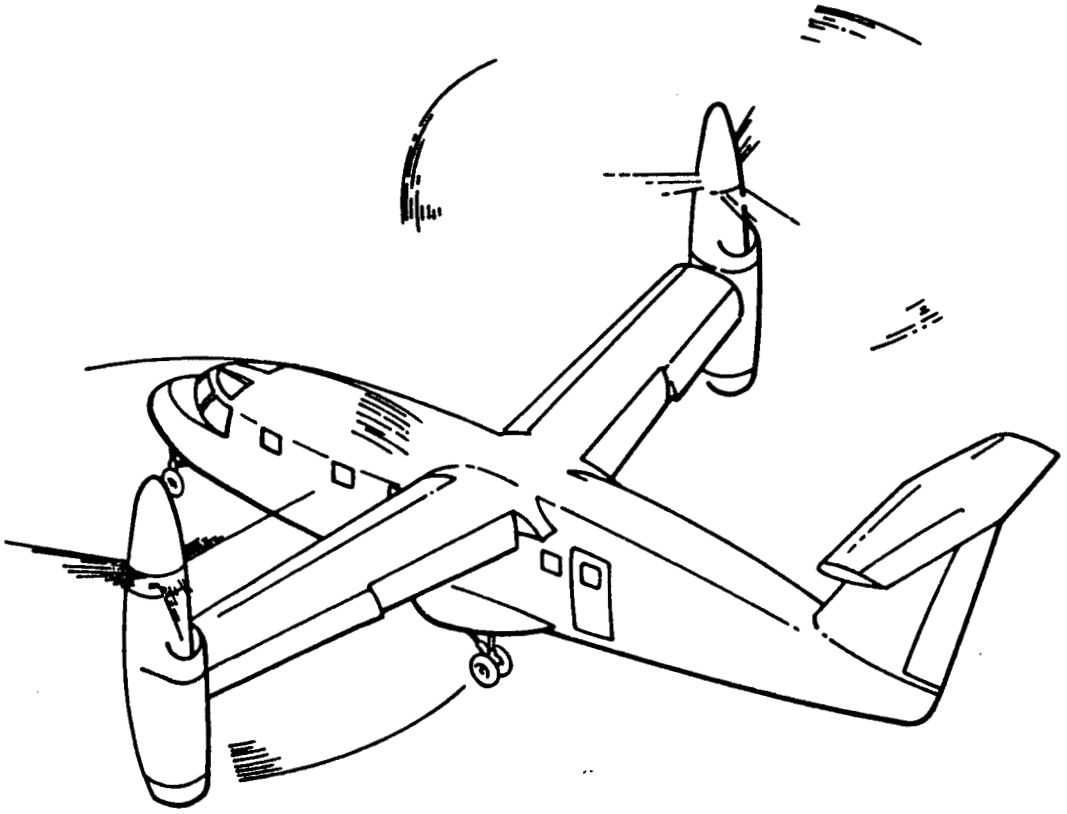

A. HOVER MODE

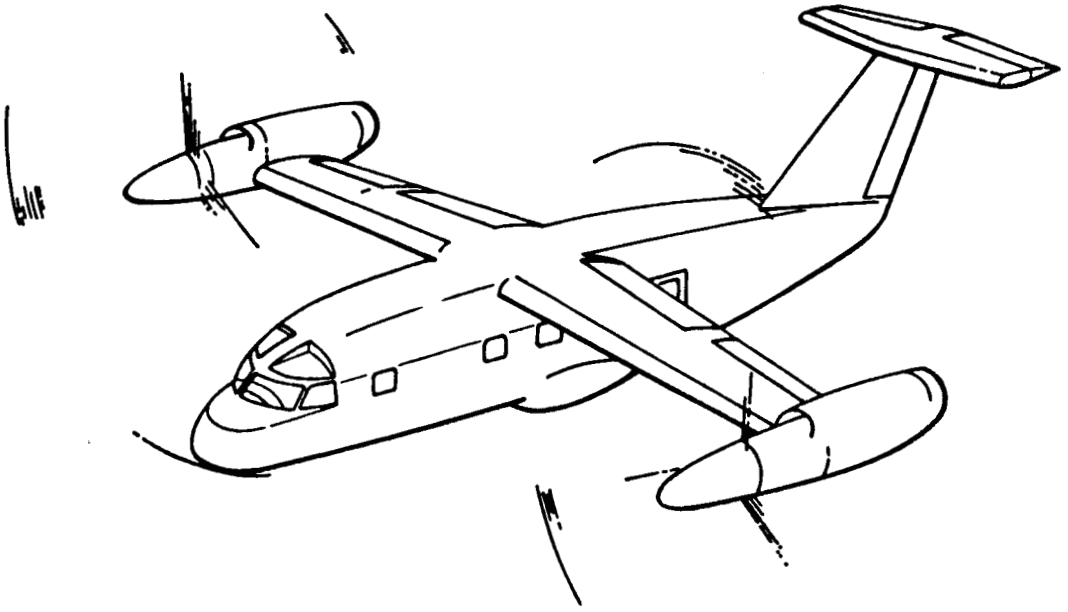

B. CRUISE MODE

Figure 1.1 The Model 266 Tilt-Rotor VTOL Transport Designed by Bell Aircraft

Guidance laws are given for take-off in Chapter IV and for landing in Chapter V. The guided aircraft behavior in the presence of initial and wind disturbances is studied in both chapters.

Chapter VI develops a mathematical model for the aircraft lateral motions. A guidance law is developed and guided aircraft behavior is studied in the presence of lateral winds.

Appendix A gives relevant data for the Bell Model 266.

Appendix B summarizes the longitudinal equations of motion and the weighting matrices used for computing guidance laws in Chapters IV and V.

CHAPTER II

Longitudinal Equations of Motion for a Tilt-Rotor VTOL Aircraft

2.1 Introduction

In order to develop guidance laws for take-off, landing and other flight conditions, it is necessary to develop a mathematical model, which is accurate enough for this purpose. Modeling aerodynamic forces is complicated by (a) the interaction between the rotor downwash and the wing, and (b) the change in configuration with rotor tilt.

The model developed here is fairly general and can be used for most tilt-rotor VTOL aircraft. The Bell Model 266 is taken as an example in our discussion. The Model 266 is a high-wing, twin engine, tilting proprotor aircraft. It has a disc loading of 58.6 Kg m^{-2} and a wing loading of 358 Kg m^{-2} at its design gross weight of 12,700 kilograms.

The two nacelles are located at the wing tips and can be rotated through slightly more than 90 degrees. Each nacelle accomodates an engine, transmission and other accessories necessary to drive a proprotor. The proprotors are similar to the rotors in a tandem rotor helicopter. Each rotor has collective pitch control and cyclic pitch control in the longitudinal and the lateral directions. The two engines are connected through an intermediate transmission so that in case of one engine failure, the two rotors can be driven at a reduced power.

A compromise is made between low disc loading for efficient hover and a high disc loading (in the propeller mode) for efficient cruise. A high wing loading is chosen to obtain good performance at cruise speed.

Some parameters of the Bell Model 266 are given in Appendix A.

2.2 Aerodynamics of the Rotor

We first develop expressions for the thrust and in-plane forces acting on the rotor and the rotor downwash under different flight conditions.

2.2.1 Thrust

The shaft horsepower required to generate a certain thrust under given flight conditions depends on the blade design. Different blade twists are required for efficient hover performance than for efficient cruise performance. In our analysis, we use a blade twist which is efficient in cruise for two reasons: (a) a twist distribution which is efficient for cruise suffers a smaller penalty in hover than vice-versa, and (b) the aircraft is in the cruise mode much longer than it is in the hover or transition mode.

The thrust available and power required at various collective pitch settings and flight conditions are obtained by using a mixture of Blade Element Theory and Momentum Theory As a first approximation, the angle between the free stream velocity and the normal to the tip path plane is assumed zero. Later analysis shows that when the free stream velocity is substantial this inflow angle is quite small. A correction can be applied for finite values of this angle. Fig. 2.1 shows a velocity diagram for a section of the blade at radius r. If R is the rotor radius and V_T the tip speed of the blades, the speed of this element of the blade is $\frac{r}{R} V_T$. Let V be the free stream velocity and v_x the induced velocity at radius r. v_x is parallel to the lift on this element. The rotor downwash is supposed to be free of rotation. Let γ_x be the twist at radius r and ϕ_c the col-

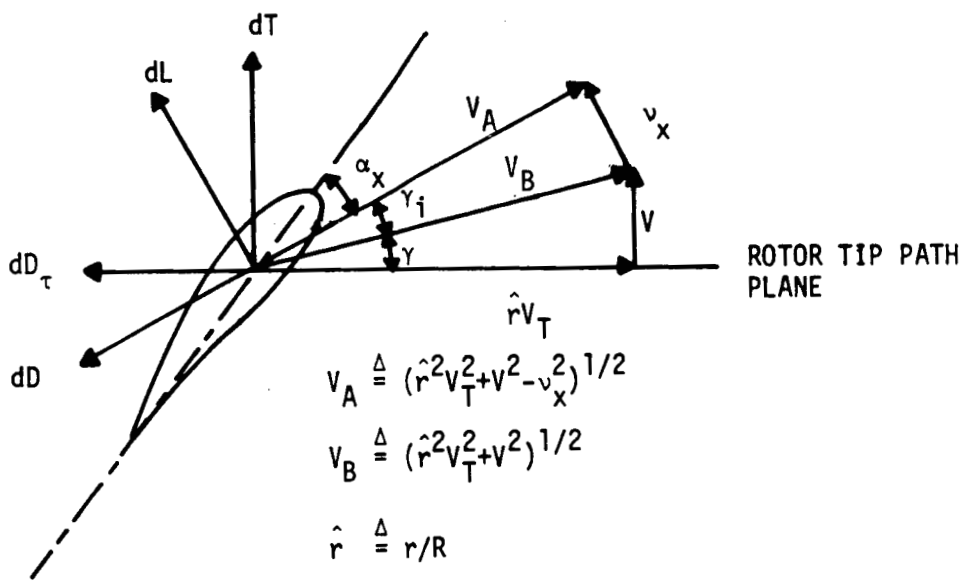

Figure 2.1 Velocity Diagram for Rotor Blade Element at Radius r

lective pitch. Then the angle of attack, α_x, on this blade element is given by

$$\alpha_x = \phi_c + \gamma_x - \gamma_i - \gamma, \tag{2.2.1}$$

where γ is the inflow angle and γ_i is the induced inflow angle. From Figure 2.1 it is clear that

$$\gamma = \arctan\left[\frac{V}{\frac{r}{R}V_T}\right] = \arctan\left(\frac{V}{\hat{r}V_T}\right) \tag{2.2.2}$$

$$\gamma_i = \arcsin\left[\frac{v_x}{((\hat{r}V_T)^2+V^2)^{1/2}}\right] \qquad (2.2.3)$$

The resultant wind speed V_R, at this blade element is given by

$$V_R^2 = (\hat{r}V_T)^2+V^2-v_x^2 \qquad (2.2.4)$$

If c is the blade chord (assumed constant), the lift, dL on this element of the blade can be determined

$$dL = \frac{1}{2}\rho C_{L_x}(\alpha_x)V_R^2\, cdr$$

$$= \frac{1}{2}\rho C_{L_x}(\alpha_x)\left\{(\hat{r}V_T)^2+V^2-v_x^2\right\} cdr \qquad (2.2.5)$$

Similarly the drag, dD on this blade element is

$$dD = \frac{1}{2}\rho\, C_{D_x}(\alpha_x)\, V_R^2\, cdr$$

$$= \frac{1}{2}\rho\, C_{D_x}(\alpha_x)\left\{(\hat{r}V_T)^2+V^2-v_x^2\right\} cdr \qquad (2.2.6)$$

If n is the number of blades, the total lift and drag produced by the section of rotor disc between radius r and r+dr can be expressed as

$$dL_D = \frac{1}{2}\rho\, ncR\, C_{L_x}(\alpha_x)\left\{(\hat{r}V_T)^2+V^2-v_x^2\right\} d(\hat{r}) \qquad (2.2.7)$$

$$dD_D = \frac{1}{2} \rho \, ncR \, C_{D_x}(\alpha_x) \left[(\hat{r}V_T)^2 + V^2 - \nu_x^2 \right] d(\hat{r}) \qquad (2.2.8)$$

Resolving these forces perpendicular and parallel to the rotor disc gives the thrust component, dT and the torque component, dD_τ, respectively:

$$dT = dL_D \cos(\gamma+\gamma_i) - dD_D \sin(\gamma+\gamma_i) \qquad (2.2.9)$$

$$dD_\tau = dL_D \sin(\gamma+\gamma_i) + dD_D \cos(\gamma+\gamma_i) \qquad (2.2.10)$$

Let B be the tip loss factor. Then the total thrust on N rotors is given by

$$T = N \int_0^{BR} dT$$

$$= \int_0^B \frac{1}{2} \rho \, ncR \, N \left\{ (\hat{r}V_T)^2 + V^2 - \nu_x^2 \right\} \left[C_{L_x}(\alpha_x) \cos(\gamma+\gamma_i) - C_{D_x}(\alpha_x) \sin(\gamma+\gamma_i) \right] d(\hat{r})$$

$$= \frac{1}{2} \rho \, ncR \, V_T^2 \, N \int_0^B \left(\hat{r}^2 + \frac{V^2}{V_T^2} - \frac{\nu_x^2}{V_T^2} \right) \cdot \left[C_{L_x}(\alpha_x) \cos(\gamma+\gamma_i) - C_{D_x}(\alpha_x) \sin(\gamma+\gamma_i) \right] d\hat{r} \qquad (2.1.11)$$

Gessow and Myers (GE-1) give a convenient expression for the tip loss factor in terms of thrust coefficient, C_T

and number of blades n

$$B = 1 - \frac{\sqrt{2C_T}}{n} \tag{2.2.12}$$

The torque produced by this section of the disc can be computed

$$d\tau = rdD_\tau$$

The total torque on one rotor is

$$\tau = \int_0^R rdD_\tau \tag{2.2.13}$$

Hence the power, Q, required to drive the N rotors at this collective pitch setting becomes

$$Q = \tau\Omega N$$

$$= \int_0^1 r\Omega \ \frac{1}{2}\rho N n c R \left[\hat{r}^2 V_T^2 + V^2 - v_x^2\right]\left[C_{L_x}(\alpha_x) \sin(\gamma+\gamma_i) + C_{D_x}(\alpha_x) \cos(\gamma+\gamma_i)\right] d\hat{r}, \tag{2.2.14}$$

where Ω is the rotational speed. Also,

$$r\Omega = \frac{r}{R} R\Omega = \hat{r}V_T$$

$$Q = \int_0^1 \tfrac{1}{2}\,\rho N n c R\, V_T \hat{r}\left[\hat{r}^2 V_T^2 + V^2 - v_x^2\right]$$

$$\cdot\left[C_{L_x}(\alpha_x)\,\sin(\gamma+\gamma_i) + C_{D_x}(\alpha_x)\,\cos(\gamma+\gamma_i)\right]d\hat{r}$$

$$= \tfrac{1}{2}\,\rho N n c R\, V_T^3 \int_0^1 \hat{r}\left(\hat{r}^2 + \frac{V^2}{V_T^2} - \frac{v_x^2}{V_T^2}\right)$$

$$\cdot\left\{C_{L_x}(\alpha_x)\,\sin(\gamma+\gamma_i) + C_{D_x}(\alpha_x)\,\cos(\gamma+\gamma_i)\right\}d\hat{r} \qquad (2.2.15)$$

Let p_x be the average pressure difference across the disc at radius r. Then,

$$p_x = \frac{dL}{d(\text{Area})} = \frac{C_{L_x}\,\frac{\rho}{2}\,ncR\,(\hat{r}^2 V_T^2 + V^2 - v_x^2)\,d\hat{r}}{2\pi r\,dr}$$

$$= \tfrac{1}{2}\,\rho\, C_{L_x}\,\frac{ncR}{2\pi R^2 \hat{r}}\,(\hat{r}^2 V_T^2 + V^2 - v_x^2) \qquad (2.2.16)$$

We can find v_x by expressing p_x in another way. By momentum theory

$$p_x = \tfrac{\rho}{2}\,(V_f^2 - V^2), \qquad (2.2.17)$$

where V_f is the maximum airspeed in the rotor downwash. Since the maximum induced velocity is twice the induced velocity at the disc [GE-1], V_f can be expressed as

$$\vec{V}_f = \vec{V} + 2\vec{v}_x$$

or,

$$V_f^2 = V^2+4v_x^2+4Vv_x \cos(\gamma+\gamma_i) \qquad (2.2.18)$$

Using equations (2.2.16) to (2.2.18), we have

$$\frac{\rho}{2}\left[4v_x^2+4Vv_x \cos(\gamma+\gamma_i)\right] = \frac{1}{2}\rho C_{L_x}\frac{ncR}{2\pi R^2\hat{r}}(\hat{r}V_T^2+V^2-v_x^2) \qquad (2.2.19)$$

$$\frac{ncR}{\pi R^2} = \sigma, \text{ solidity ratio}$$

$$v_x^2\left[1+\frac{C_{L_x}\sigma}{8\hat{r}}\right] + v_xV\cos(\gamma+\gamma_i) - \frac{C_{L_x}\sigma}{8\hat{r}}[\hat{r}^2V_T^2+V^2] = 0 \qquad (2.2.20)$$

This equation can be solved for v_x at each radius.

The following expressions were used for the lift coefficient and the drag coefficient on any blade section.

$$C_{L_x} = 6.0\,\alpha_x \qquad |\alpha_x| < \frac{1}{4} \qquad (2.2.21)$$

$$|\alpha_x| > \frac{1}{4} \text{ not allowed (stall condition)}$$

$$C_{D_x} = .008 - .008\,C_{L_x} + .020\,C_{L_x}^2 \qquad (2.2.22)$$

2.2.2 Computation of In-Plane Forces

In almost all flight conditions considered here the component of in-plane force in the forward direction is very

small. This force has a significant effect only during high speed flight in the helicopter mode. Thus, for purposes of this analysis, it will be sufficient to determine this force approximately. It is computed by taking an average drag coefficient C_{D_B} on the blade. The drag on an element of the blade between radius r and r+dr situated at azimuth angle ψ from down wind position is (Figure (2.2)):

$$dD = \frac{1}{2}\rho\left(\frac{r}{R}V_T + V \sin\psi \cos\phi\right)^2 c\,dr\,C_{D_B} \qquad (2.2.23)$$

Its component in the downwind direction is,

$$dH = \frac{1}{2}\rho\left(\frac{r}{R}V_T + V \sin\psi \cos\phi\right)^2 c\,dr\,C_{D_B} \sin\psi \qquad (2.2.24)$$

Average total drag on all blades can now be determined.

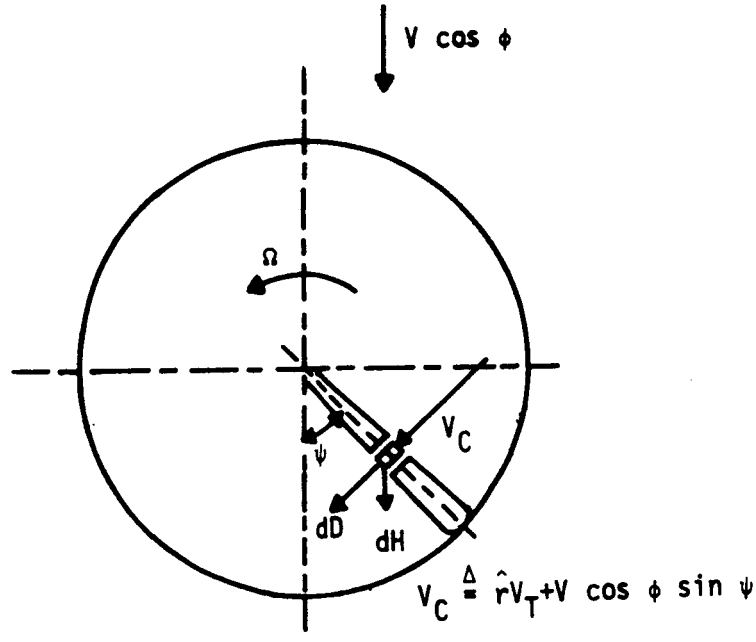

Figure 2.2 In-Plane Forces on a Blade Element

$$H = \frac{1}{2\pi}\int_0^{2\pi}\int_0^R n \frac{1}{2} \rho c dr \, C_{D_B} \sin \psi$$

$$\cdot\left(\frac{r}{R} V_T + V \sin \psi \cos \phi\right)^2 d\psi$$

$$= \int_0^1 \frac{1}{2} \rho \, ncR \, C_{D_B} \left(\frac{2\hat{r}V_T \, V \cos \phi}{2}\right) d\hat{r}$$

$$= \frac{1}{2} \rho \, ncR \, C_{D_B} \frac{V_T V \cos \phi}{2} \qquad (2.2.25)$$

Hence drag force on N rotors is,

$$H = \frac{1}{4} \rho \, \sigma \, N\pi R^2 \, C_{D_B}(V_T V \cos \phi) \qquad (2.2.26)$$

This is an approximate formula and corresponds to the first term in equation (4.38) of Nikolsky (NI-1)

2.2.3 Induced Velocity

The computation of wing drag and lift requires knowledge of rotor downwash. The downwash velocity depends on the radial distance from the axis of rotation and distance perpendicular to the tip path plane. To simplify calculation of lift and drag over the wing in the next section, the induced velocity over that part of the wing immersed in rotor downwash is assumed to be constant and equal to the maximum induced velocity. Using momentum theory this velocity is 2ν where ν is obtained by solving the equation (GE-1),

$$\nu[V^2+\nu^2+2V\nu \cos \phi]^{1/2} = \frac{T}{N \, 2\pi R^2 \, \rho} \quad . \qquad (2.2.27)$$

2.2.4 Thrust for the Example Aircraft

A computer program was written to determine the maximum available thrust at rated power. Figure 2.3 shows the variation of thrust with inflow velocity. For nonzero

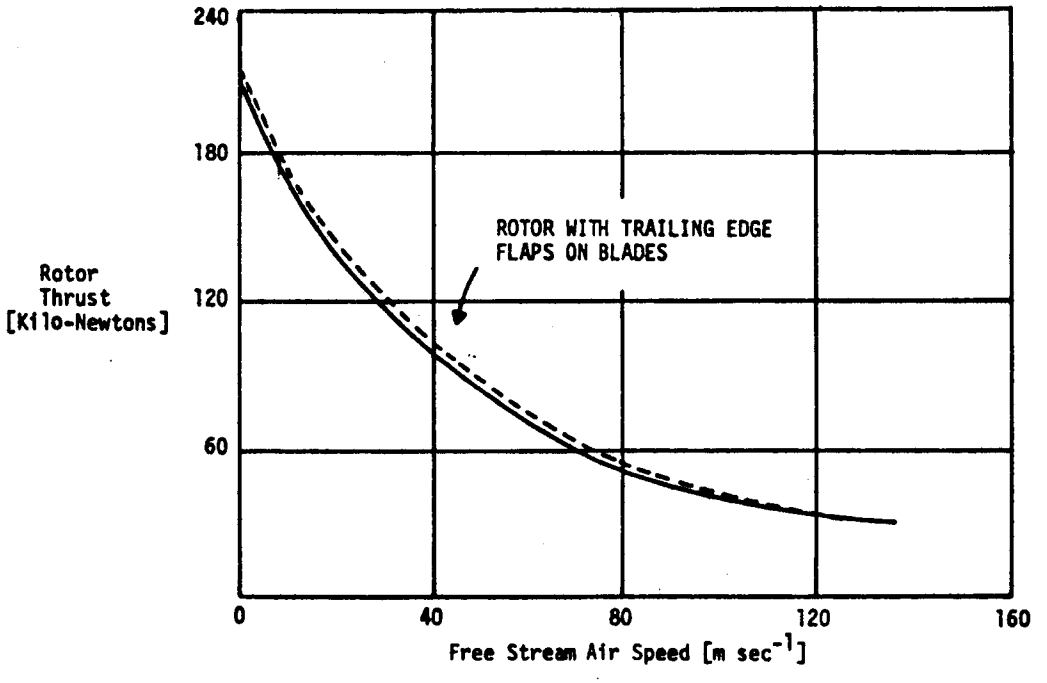

Figure 2.3 Variation of Rotor Thrust with Free Stream Air Speed

values of inflow angle, the component of velocity in the direction normal to the tip path plane is used to read thrust from Figure 2.3. This gives conservative results.

At least one author (HA-1) has suggested using trailing edge flaps on the blades to obtain almost optimal twist distribution along the blade under all flight conditions. The maximum available thrust for a rotor with blades having trailing edge flaps is shown in Figure 2.3 (dotted line). The maximum increase is about 4.5% over a rotor with flapless blades. Notice that both perform equally well at cruise. The rotor with blade flaps performs better during hover. Such a minor improvement in performance with flaps does not seem to warrant the additional mechanical complication.

2.3 Equations of Motion in Forward and Vertical Directions

The forces acting on a tilt rotor VTOL aircraft can be divided into two classes: (a) gravitational and (b) aerodynamic. The aerodynamic forces can be subdivided into two classes: (i) forces with all control elements in equilibrium position and (ii) additional forces generated by deflecting control surfaces. Gravitational forces are quite easy to find. The aerodynamic forces are approximated by sums of forces on individual components of the aircraft.

A simplified force diagram is shown in Figure 2.4. Let D be the drag and L the lift. The thrust and the in-plane force on the rotor are denoted by T and H respectively. The equations of motion parallel and perpendicular to the velocity of the vehicle mass center can be written as

$$m \frac{dV}{dt} = -D - mg \sin \gamma + T \cos (\eta+\theta-\gamma) - H \sin (\eta+\theta-\gamma) \qquad (2.3.1)$$

$$mV \frac{d\gamma}{dt} = +L-mg \cos \gamma +T \sin (\eta+\theta-\gamma)+H \cos (\eta+\theta-\gamma) \quad (2.3.2)$$

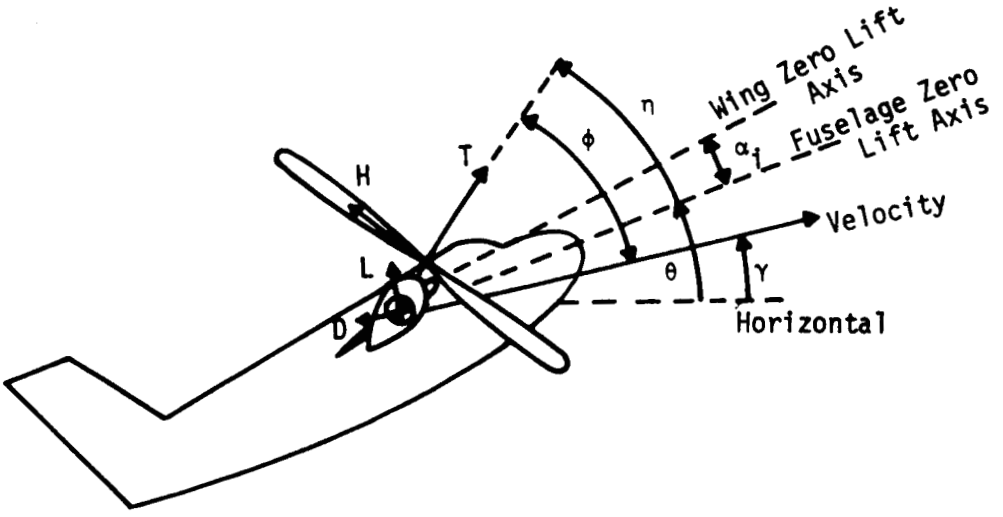

Figure 2.4 Aircraft Reference Angles and Forces

The drag and lift are expressed as sums of forces on individual components.

$$D = D_W + D_T + D_F + D_{NAC} \quad (2.3.3)$$

$$L = L_W + L_T + L_F + L_{NAC} \quad (2.3.4)$$

We consider these aircraft components one by one.

2.3.1 Wing

The wing of a tilt-rotor VTOL airplane will usually have flaps and aileron-flaps. These flaps can be deflected through 60° or more during hover to reduce wing surface in the rotor downwash. The ailerons can also be used as flaps during hover and part of transition.

A portion of the wing is in the rotor downwash. This has a significant effect during hover and the early part of transition where the induced velocity is high. It is assumed that the portion of the wing under the rotor disc is in the rotor downwash and faces a constant induced velocity. This induced velocity over the immersed part of the wing is approximated by the fully developed downstream velocity in the slipstream. Let ϵ be the fraction of the wing in rotor downwash. This portion is denoted by subscript 1 and the other part by subscript 2.

The angle of attack α over the portion of the wing in the free stream is given as

$$\alpha = \theta + \alpha_i - \gamma \tag{2.3.5}$$

The flaps change the effective angle of attack. Let the effective angle of attack be α'.

$$\alpha' = \alpha + \Delta\alpha_f(\delta f)$$

$$\tilde{-} \alpha + g_f \, \delta f \tag{2.3.6}$$

where δf is the flap deflection. The lift coefficient depends on α' and the drag coefficient on α and δf.

$$D_{W_2} = \frac{1}{2} \rho \, C_{D_W}(\alpha, \delta f) \, V^2 \, S_W \, (1-\epsilon) \tag{2.3.7}$$

$$L_{W_2} = \frac{1}{2} \rho \, C_{L_W}(\alpha') \, V^2 \, S_W \, (1-\epsilon) \tag{2.3.8}$$

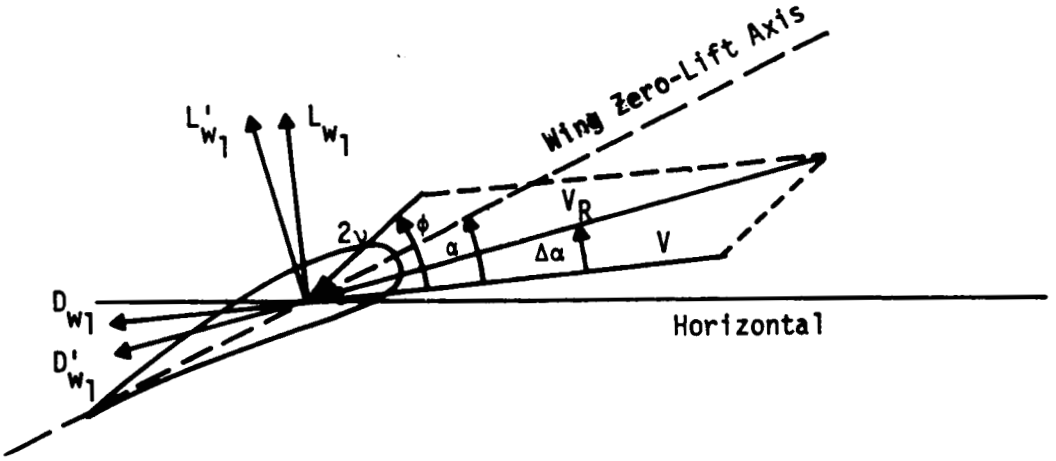

Figure 2.5 Velocity Diagram over Immersed Part of Wing

The downwash changes the magnitude and the direction of velocity. A simplified velocity diagram over the immersed portion of the wing is shown in Figure 2.5. The resultant velocity, V_R, can be computed.

$$V_R^2 = V^2 + 4\nu^2 + 4V\nu \cos \phi \qquad (2.3.9)$$

The change in angle of attack, $\Delta\alpha$, is obtained using the Sine Law of triangles.

$$\frac{\sin (\Delta\alpha)}{2\nu} = \frac{\sin \phi}{V_R}$$

where,

$$\phi = \eta+\theta-\gamma \qquad (2.3.10)$$

hence,

$$\Delta\alpha = \arcsin\left\{\frac{2\nu}{V_R}\sin(\phi)\right\} \tag{2.3.11}$$

The resultant angle of attack α_R is written as,

$$\alpha_R = \alpha - \Delta\alpha \tag{2.3.12}$$

Now the forces on the wing along the direction of V_R, $D_{W_1}^{V_R}$, and perpendicular to the direction of V_R, $L_{W_1}^{V_R}$, are given by

$$D'_{W_1} = \frac{1}{2}\rho\, C_{D_W}(\alpha_R, \delta f)\, V_R^2\, S_W\, \epsilon \tag{2.3.13}$$

$$L'_{W_1} = \frac{1}{2}\rho\, C_{L_W}(\alpha' - \Delta\alpha)\, V_R^2\, S_W\, \epsilon \tag{2.3.14}$$

These forces must be resolved along the direction of the free stream velocity and perpendicular to this direction to give D_{W_1} and L_{W_1}.

$$\begin{aligned} D_{W_1} &= D'_{W_1}\cos(\Delta\alpha) + L'_{W_1}\sin(\Delta\alpha) \\ &= \frac{1}{2}\rho\, V_R^2\, S_W\, \epsilon\, [C_{D_W}(\alpha_R, \delta f)\cos(\Delta\alpha) \\ &\quad + C_{L_W}(\alpha' - \Delta\alpha)\sin\Delta\alpha] \end{aligned} \tag{2.3.15}$$

$$L_{W_1} = -D'_{W_1} \sin(\Delta\alpha) + L'_{W_1} \cos(\Delta\alpha)$$

$$= \frac{1}{2} \rho V_R^2 S_W \varepsilon [-C_{D_W}(\alpha_R, \delta f) \sin(\Delta\alpha)$$

$$+C_{L_W}(\alpha'-\Delta\alpha) \cos(\Delta\alpha)] \qquad (2.3.16)$$

The total drag on the wing can be written as,

$$D_W = D_{W_1}+D_{W_2}$$

$$L_W = L_{W_1}+L_{W_2} \qquad (2.3.17)$$

Determination of Drag Coefficient and Lift Coefficient

The flight regime of a tilt-rotor VTOL aircraft encompasses angles of attack varying from -90° to 90° or more. These high angles of attack occur at low speeds, during take-off and during landing. Most of the high speed flight takes place at low angles of attack with most or all of the weight carried by the wing. A large error in drag coefficient and lift coefficient at these high angles of attack will produce only a small error in the forces acting on the airplane because of low velocity. Therefore it is not necessary to have very accurate relations for C_{D_W} and C_{L_W} for high positive or negative angles of attack.

It is essential to find the positive and the negative angle of attack at which wing stall occurs. We suppose that with no flap deflection the stall occurs at angle of attack $\pm \alpha_{stall}$. The flap deflection increases the effective angle of attack. It also increases the effective

angle of attack at which stall occurs. In terms of actual angle of attack the stall starts earlier because flap deflection helps flow separation near the trailing edge. The actual positive and negative angles of attack at which stall occurs is approximated by using Figure 12 of reference (BE-1)

$$\alpha_s^+ = \alpha_{stall} - \frac{g_f \delta f}{2} \qquad (2.3.18)$$

$$\alpha_s^- = -\alpha_{stall} - \frac{g_f \delta f}{2} \qquad (2.3.19)$$

The effective angle of attack α' is given by equation (2.3.12). In terms of this angle the stall condition can be written as

$$\alpha_s'^+ = \alpha_{stall} + \frac{g_f \delta f}{2} \qquad (2.3.20)$$

$$\alpha_s'^- = -\alpha_{stall} + \frac{g_f \delta f}{2} \qquad (2.3.21)$$

During the unstalled part of the flight a linear relation is assumed between the lift coefficient and the effective angle of attack, i.e.,

$$C_L(\alpha') = a\alpha' \qquad \alpha_s'^- < \alpha' < \alpha_s'^+ \qquad (2.3.22)$$

As the angle of attack increase above α_s^+ the lift coefficient decreases. At a certain high angle of attack the lift coefficient becomes zero. This angle is approximately 90° with no flap deflection but decreases with positive flap deflection. It is reasonable to assume that the

lift coefficient is zero when the net projected area in the lateral direction is zero (Figure 2.6).

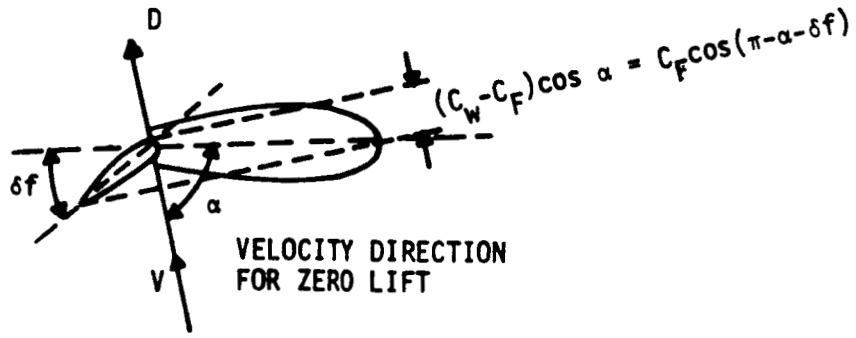

Figure 2.6 Zero Lift Angle of Attack

Thus,

$$C_L(\alpha') = 0 \qquad \tan\left(\frac{\pi}{2} - \alpha\right) = \frac{C_f \sin \delta f}{C_W - C_f(1-\cos \delta f)}$$

and a similar expression for negative angles of attack

$$C_L(\alpha') = 0 \qquad \tan\left(\frac{\pi}{2} - \alpha\right) = -\frac{C_f \sin \delta f}{C_W - C_f(1-\cos \delta f)}$$

These equations are approximated for $\alpha \simeq \pm \frac{\pi}{2}$,

$$C_L(\alpha') = 0 \qquad \alpha = \pm \frac{\pi}{2} - \frac{C_f}{C_W}\delta f \qquad (2.3.23)$$

A linear relation is assumed between lift coefficient and angle of attack for α between stall angle and angle at which the lift coefficient is zero. Therefore,

$$C_L(\alpha') = a\alpha' \qquad \alpha_s'^- \leq \alpha' \leq \alpha_s'^+$$

$$= \frac{a\alpha_s'^+ \left[\frac{\pi}{2} - \frac{C_f}{C_w}\delta f + g_f\delta f - \alpha'\right]}{\left[\frac{\pi}{2} - \frac{C_f}{C_w}\delta f + g_f\delta f - \alpha_s'^+\right]} \qquad \alpha' > \alpha_s'^+$$

$$= \frac{a\alpha_s'^- \left[\frac{\pi}{2} + \frac{C_f}{C_w}\delta f + \alpha' - g_f\delta f\right]}{\left[\frac{\pi}{2} + \frac{C_f}{C_w}\delta f + \alpha_s'^- - g_f\delta f\right]} \qquad \alpha' < \alpha_s'^- \tag{2.3.24}$$

A plot of lift coefficient with angle of attack for no flap deflection and for one radian flap deflection is shown in Figure 2.7.

In the unstalled regime the drag coefficient is given by

$$C_{D_W}(\alpha',\delta f) = C_{D_{W_0}}(\delta f) + C_{D_{W_1}} C_L^2 \qquad \alpha_s'^- \leq \alpha' \leq \alpha_s'^+$$

$$= C_{D_{W_0}}(\delta f) + C_{D_{W_1}} \alpha'^2 a^2 \tag{2.3.25}$$

The first term is the parasite drag which depends upon the flap deflection and the second term is the induced drag. A good approximation to the first term is (PE-1)

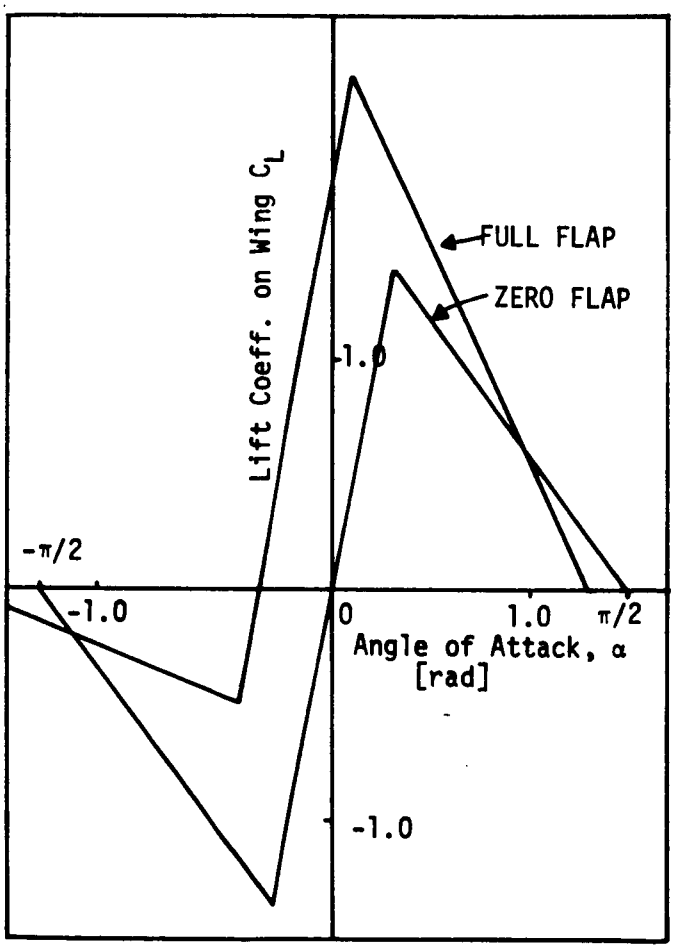

Figure 2.7 Lift Coefficient vs. Angle of Attack on Wing

$$C_{D_{W_0}}(\delta f) = \beta_1 + \beta_2(\delta f)^2$$

In the stalled regime the lift reduces; however the drag keeps increasing. The following expressions are used for drag coefficients for the stalled portion of the flight.

$$C_D(\alpha',\delta f) = C_{D_{W_0}}(\delta f)+C_{D_{W_1}} C_{L_{max}}^2 +\beta_3(\alpha'-\alpha_s'^{+})$$

$$\alpha' > \alpha_s'^{+}$$

$$= C_{D_{W_0}}(\delta f)+C_{D_{W_1}} C_{L_{max}}^2 +\beta_3(\alpha_s'^{-}-\alpha')$$

$$\alpha' < \alpha_s'^{-}$$

The expression for $C_D(\alpha',\delta f)$ can be summed up as

$$C_D(\alpha',\delta f) = \beta_1+\beta_2\delta f^2+C_{D_{W_1}} a^2\alpha_s'^{-2}+\beta_3(\alpha_s'^{-}-\alpha')$$

$$\alpha' < \alpha_s'^{-}$$

$$= \beta_1+\beta_2\delta f^2+C_{D_{W_1}} a^2\alpha'^2$$

$$\alpha_s'^{-} \leq \alpha' \leq \alpha_s'^{+}$$

$$= \beta_1+\beta_2\delta f^2+C_{D_{W_1}} a^2\alpha_s'^{+2}+\beta_3(\alpha'-\alpha_s'^{+})$$

$$\alpha' > \alpha_s'^{+}$$

(2.3.26)

In Figure 2.8 drag coefficient is shown as a function of angle of attack, α, for zero and maximum flap deflections. Lift coefficient is shown as a function of drag coefficient in Figure 2.9.

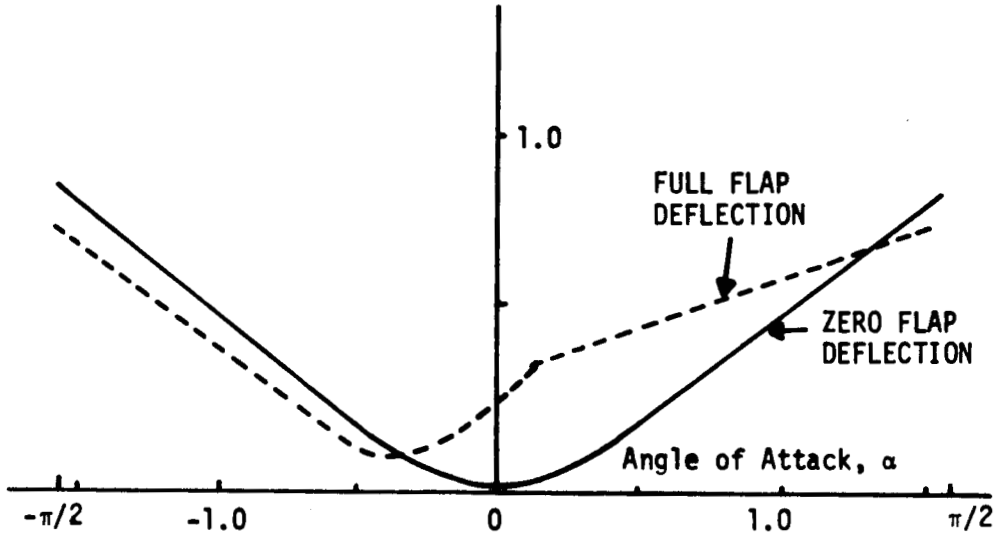

Figure 2.8 C_D vs. α on Wing

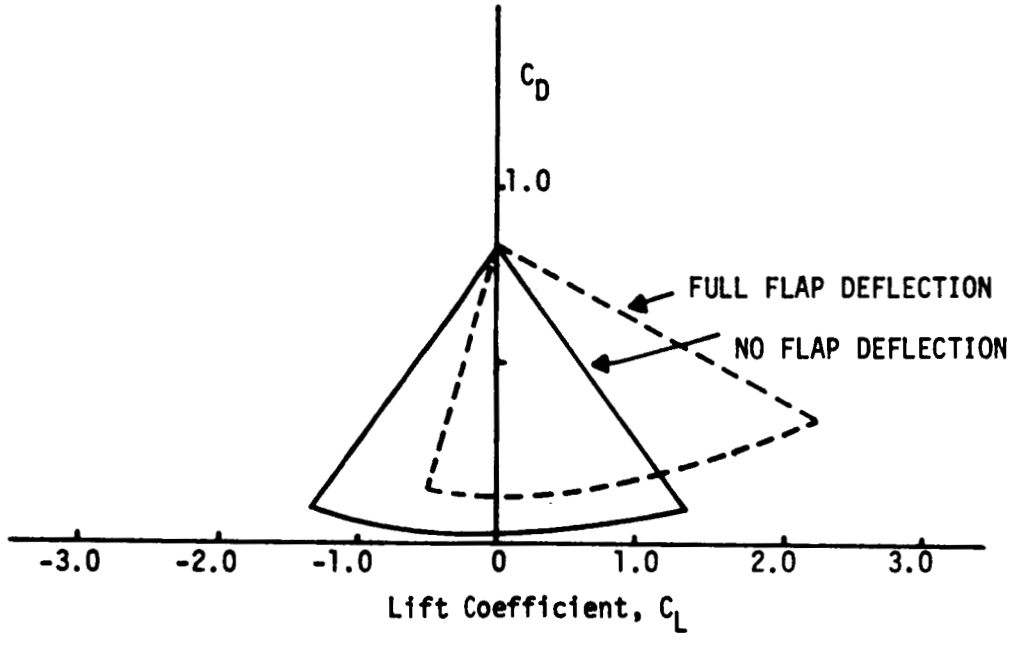

Figure 2.9 Lift Coefficient vs. Drag Coefficient on Wing

2.3.2 Tail

During most of the flight regime under consideration the rotor downwash does not have a significant effect on flow over the tail. In hover or when the forward speed is low, the induced velocity is high. Under such conditions the downwash is pointing almost vertically downward and does not pass over the tail. When the forward speed is high and the transition is over the induced velocity is so low that it does not produce any significant effect on the tail.

We use drag and lift values on the tail for zero elevator deflection. The direct effect of elevator deflection on vehicle lift and drag is neglected. The indirect effect through change in angle of attack on the wing is important.

The angle of attack on the tail is

$$\alpha_T = \theta - \gamma + \alpha_{iT} \tag{2.3.26}$$

where α_{iT} is the angle of incidence of the tail. The lift and drag coefficient on the tail are assumed to have expressions similar to wing, i.e.,

$$C_{L_T}(\alpha_T) = a_T \alpha_T \qquad |\alpha_T| \leq \alpha_{sT}$$

$$= \frac{a_T \alpha_{sT}\left[\frac{\pi}{2} - \alpha_T\right]}{\left[\frac{\pi}{2} - \alpha_{sT}\right]} \qquad \alpha_T > \alpha_{sT}$$

$$= -\frac{a_T \alpha_{sT}\left[\frac{\pi}{2} + \alpha_T\right]}{\left[\frac{\pi}{2} - \alpha_{sT}\right]} \qquad \alpha_T < -\alpha_{sT} \tag{2.3.27}$$

$$C_{D_T} = C_{D_{T_0}} + C_{D_{T_1}} a_T^2 \alpha_T^2 \qquad |\alpha_T| \leq \alpha_{sT}$$

$$= C_{D_{T_0}} + C_{D_{T_1}} a_T^2 \alpha_{sT}^2 + \beta_{3_T}(\alpha_T - \alpha_{sT}) \qquad \alpha_T > \alpha_{sT}$$

$$= C_{D_{T_0}} + C_{D_{T_1}} a_T^2 \alpha_{sT}^2 + \beta_{3_T}(-\alpha_{sT} - \alpha_T) \qquad \alpha_T < -\alpha_{sT} \tag{2.3.28}$$

The drag and the lift on the tail are given by

$$L_T = \frac{1}{2} \rho V^2 S_T C_{L_T} \tag{2.3.29}$$

$$D_T = \frac{1}{2} \rho V^2 S_T C_{D_T} \tag{2.3.30}$$

2.3.3 Fuselage

The lift and drag on the fuselage depends on the shape of the fuselage in addition to the fuselage angle of attack. The fuselage is approximated by a long cylinder. The drag coefficient and lift coefficient can be written as (HO-1)

$$C_{D_F} = C_{D_{F_1}} \sin^3 |\alpha_F| + C_{D_{F_0}} \tag{2.3.31}$$

$$C_{L_F} = C_{L_{F_1}} \sin^2 \alpha_F \cos \alpha_F \operatorname{sgn}(\alpha_F) \tag{2.3.32}$$

The lift coefficient and drag coefficient are shown in Figure 2.10 as a function of the fuselage angle of attack, α_F, given by

$$\alpha_F = \theta - \gamma \tag{2.3.33}$$

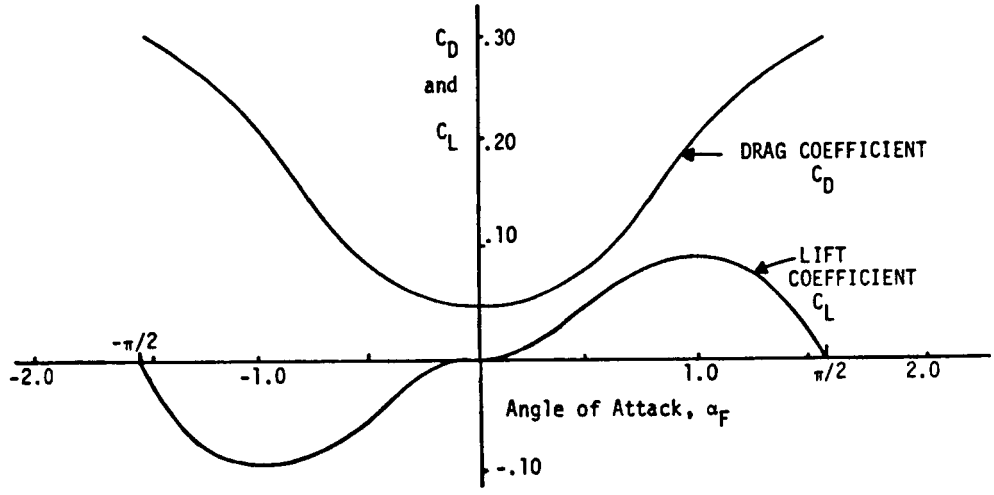

Figure 2.10 Lift and Drag Coefficients on the Fuselage

If S_F is the fuselage platform area, the lift and the drag can be written as,

$$D_F = \frac{1}{2} \rho V^2 S_F C_{D_F}(\alpha_F) \qquad (2.3.34)$$

$$L_F = \frac{1}{2} \rho V^2 S_F C_{L_F}(\alpha_F) \qquad (2.3.35)$$

2.3.4 Nacelles

The nacelles are completely immersed in rotor downwash under all flight conditions. They are also approximated by long cylinders. The lift and drag coefficients of equations (2.3.31) and (2.3.32) can then be used. If S_{NAC} is the platform area of the two nacelles, the drag and lift are

given by

$$D_{NAC} = \frac{1}{2} \rho V_R^2 S_{NAC} C_{D_{NAC}}(\alpha_{NAC}) \qquad (2.3.36)$$

$$L_{NAC} = \frac{1}{2} \rho V_R^2 S_{NAC} C_{L_{NAC}}(\alpha_{NAC}) \qquad (2.3.37)$$

where V_R is given by equation (2.3.4) and α_{NAC} is the nacelle angle of attack.

$$\alpha_{NAC} = \eta + \alpha_F - \Delta\alpha \qquad (2.3.38)$$

CHAPTER III
Tilt-Rotor VTOL Aircraft Guidance

3.1 Introduction

The requirement for a good guidance scheme for near terminal operations of a VTOL aircraft was discussed in Chapter I. The scheme should be as simple as possible so that a small airborne computer can handle it. We have adopted the perturbation guidance scheme because of the simple linear feedback law that it gives. This method consists of linearizing the nonlinear state equations about a nominal path. The feedback control gains are obtained by using this linearized system of equations and suitably chosen weighting matrices in the quadratic synthesis technique.

The equations of motion in the vertical plane are derived in Chapter II. They are,

$$\frac{dV}{dt} = F_1(V,\gamma;\theta,n,T,\delta f) \qquad (3.1.1)$$

$$V\frac{d\gamma}{dt} = F_2(V,\gamma;\theta,n,T,\delta f) \qquad (3.1.2)$$

$$\frac{dh}{dt} = V \sin\gamma \qquad (3.1.3)$$

$$\frac{dx}{dt} = V \cos\gamma \qquad (3.1.4)$$

The symbols have the same meaning as in Chapter II.

Under almost all flying conditions it is possible to generate large control moments. In the helicopter mode pitching moment is produced by dual longitudinal cyclic pitch change, yawing moment by differential shaft tilt of the two rotors (or by differential longitudinal cyclic pitch change), and rolling moment by differential collective pitch change. In the cruise mode control moments can be produced using the regular aerodynamic surfaces or cyclic and collective pitch changes. Because of large available pitch moment generating capability it is possible to put a tight control on the pitch angle. under these conditions, the pitching motions occur in a frequency range very much higher than the frequency range of the translational motions governed by equations (3.1.1-4). Therefore the translational motion equations can be decoupled from the angular motion equations and θ can be taken as a control variable for the translational motion. In this system, V, γ, x and h are state variables and θ, η, T and δf are control variables. Since none of the equations depend explicitly on t, we can use x as the independent variable.* The equations of motion then become,

$$\frac{dV}{dx} = \frac{F_1}{V \cos \gamma} = f_1 \qquad (3.1.5)$$

$$\frac{d\gamma}{dx} = \frac{F_2}{V^2 \cos \gamma} = f_2 \qquad (3.1.6)$$

$$\frac{dh}{dx} = \tan \gamma \qquad (3.1.7)$$

*Later we shall use h as the independent variable during the vertical and near-vertical part of the take-off.

If time, t is required it can be obtained by solving

$$\frac{dt}{dx} = \frac{1}{V \cos \gamma} \qquad (3.1.8)$$

3.2 Linearizing of the Equations of Motion

The guidance scheme must work in the presence of steady or fluctuating winds. Therefore, it is necessary to distinguish between air speed and ground speed (see Figure 3.1).* The air values are represented by subscript "a" and ground values by subscript "g". Nominal values are represented by a bar. In the presence of wind the lift and the drag do not act perpendicular and parallel to the ground velocity. The equations of motion must be modified to

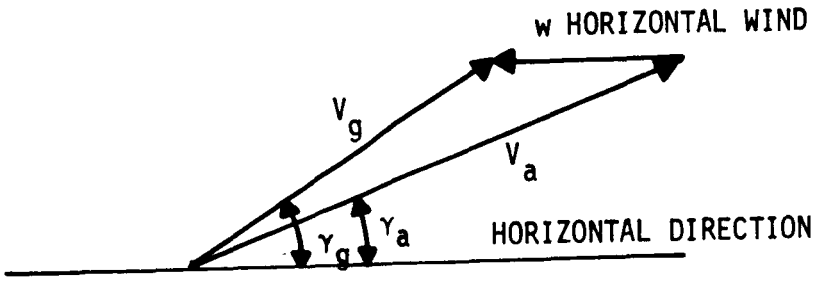

Figure 3.1 Ground and Air Speed in the Presence of Wind

*Near the ground vertical winds are negligible compared to horizontal winds

$$\frac{dV_g}{dx} = \left\{F_1(V_a,\gamma_a,\theta,n,T,\delta f)\cos(\gamma_a-\gamma_g)\right\}$$

$$-F_2(V_a,\gamma_a,\theta,n,T,\delta f)\sin(\gamma_a-\gamma_g)\Big\}/(V_g\cos\gamma_g)$$

$$\triangleq \left\{F_{1a}\cos(\gamma_a-\gamma_g)-F_{2a}\sin(\gamma_a-\gamma_g)\right\}/(V_g\cos\gamma_g) \tag{3.2.1}$$

$$\frac{d\gamma_g}{dx} = \frac{1}{V_g^2\cos\gamma_g}\left\{F_{2a}\cos(\gamma_a-\gamma_g)+F_{1a}\sin(\gamma_a-\gamma_g)\right\} \tag{3.2.2}$$

$$\frac{dh}{dx} = \tan\gamma_g \tag{3.2.3}$$

where

$$V_a^2 = V_g^2+w^2+2V_g w\cos\gamma_g$$

$$\sin\gamma_a = \frac{V_g}{V_a}\sin\gamma_g$$

If equations governing nominal values of ground speed, flight path angle and vertical distance (where wind is zero) are subtracted from the above equations, we have

$$\frac{dV_g}{dx} - \frac{d\bar{V}_g}{dx} = [F_{1a}\cos(\gamma_a-\gamma_g)-F_{2a}\sin(\gamma_a-\gamma_g)]/(V_g\cos\gamma_g)$$

$$-F_1(\bar{V}_g,\bar{\gamma}_g,\bar{\theta},\bar{n},\bar{T},\bar{\delta f})/\bar{V}_g\cos\bar{\gamma}_g]$$

$$= [F_{1a}\cos(\gamma_a-\gamma_g)-F_{2a}\sin(\gamma_a-\gamma_g)]/(V_g\cos\gamma_g)$$

$$-\frac{F_{1g}}{V_g\cos\gamma_g} + \frac{F_{1g}}{V_g\cos\gamma_g} - \frac{F_{1\bar{g}}}{\bar{V}_g\cos\bar{\gamma}_g}$$

$$= \frac{\{F_{1a}\cos(\gamma_a-\gamma_g)-F_{2a}\sin(\gamma_a-\gamma_g)-F_{1g}\}}{V_g\cos\gamma_g}$$

$$+ \frac{F_{1g}}{V_g\cos\gamma_g} - \frac{F_{1\bar{g}}}{\bar{V}_g\cos\bar{\gamma}_g} \qquad (3.2.4)$$

The first term represents the effect of wind and the second term the deviation of the state and control variables from nominal values. Now

$$\frac{F_{1g}}{V_g\cos\gamma_g} - \frac{F_{1\bar{g}}}{\bar{V}_g\cos\bar{\gamma}_g} \triangleq f_{1g}-f_{1\bar{g}}$$

$$\simeq \left.\frac{\partial f_{1g}}{\partial V_g}\right|_{\bar{g}} \delta V_g + \left.\frac{\partial f_{1g}}{\partial \gamma_g}\right|_{\bar{g}} \delta\gamma_g + \left.\frac{\partial f_{1g}}{\partial \theta}\right|_{\bar{g}} \delta\theta$$

$$+ \left.\frac{\partial f_{1g}}{\partial \eta}\right|_{\bar{g}} \delta\eta + \left.\frac{\partial f_{1g}}{\partial T}\right|_{\bar{g}} \delta T + \left.\frac{\partial f_{1g}}{\partial(\delta f)}\right|_{\bar{g}} \delta(\delta f), \qquad (3.2.5)$$

for small changes.

The first term in (3.2.4) can be simplified as,

$$\frac{F_{1a}\cos(\gamma_a-\gamma_g)-F_{2a}\sin(\gamma_a-\gamma_g)-F_{1g}}{V_g\cos\gamma_g}$$

$$\simeq \frac{F_{1a}-F_{1g}-F_{2a}(\gamma_a-\gamma_g)}{V_g\cos\gamma_g} \qquad (3.2.6)$$

$$\simeq \frac{1}{V_g\cos\gamma_g}\left[\frac{\partial F_{1g}}{\partial V_g}\frac{\partial V_a}{\partial w} + \frac{\partial F_{1g}}{\partial \gamma_g}\frac{\partial \gamma_a}{\partial w} - F_{2g}\frac{\partial \gamma_a}{\partial w}\right] w$$

where w is the wind velocity. Since

$$F_{1g} = f_{1g} V_g \cos \gamma_g$$

$$\frac{\partial F_{1g}}{\partial V_g} = \frac{\partial f_{1g}}{\partial V_g} V_g \cos \gamma_g + f_{1g} \cos \gamma_g \qquad (3.2.7)$$

$$\frac{\partial F_{1g}}{\partial \gamma_g} = \frac{\partial f_{1g}}{\partial \gamma_g} V_g \cos \gamma_g - f_{1g} V_g \sin \gamma_g \qquad (3.2.8)$$

Therefore,

$$\frac{F_{1a}\cos(\gamma_a-\gamma_g)-F_{2a}\sin(\gamma_a-\gamma_g)-F_{1g}}{V_g \cos \gamma_g}$$

$$\simeq \left\{ \left(\frac{\partial f_{1g}}{\partial V_g} + \frac{f_{1g}}{V_g} \right) \frac{\partial V_a}{\partial w} \right.$$

$$\left. + \left(\frac{\partial f_{1g}}{\partial \gamma_g} - f_{1g} \tan \gamma_g - f_{2g} V_g \right) \frac{\partial \gamma_a}{\partial w} \right\} w \qquad (3.2.9)$$

hence equation (3.2.4) becomes,

$$\frac{d\delta V_g}{dx} = \frac{\partial f_{1g}}{\partial V_g} \delta V_g + \frac{\partial f_{1g}}{\partial \gamma_g} \delta \gamma_g + \frac{\partial f_{1g}}{\partial \theta} \delta\theta$$

$$+ \frac{\partial f_{1g}}{\partial \eta} \delta\eta + \frac{\partial f_{1g}}{\partial T} \delta T + \frac{\partial f_{1g}}{\partial \delta f} \delta(\delta f)$$

$$+ \left\{ \left(\frac{\partial f_{1g}}{\partial V_g} + \frac{f_{1g}}{V_g} \right) \frac{\partial V_a}{\partial w} \right.$$

$$\left. + \left(\frac{\partial f_{1g}}{\partial \gamma_g} - f_{1g} \tan \gamma_g - V_g f_{2g} \right) \frac{\partial \gamma_a}{\partial w} \right\} w \qquad (3.2.10)$$

$$\frac{d(\delta\gamma_g)}{dx} = \frac{\partial f_{2g}}{\partial V_g}\delta V_g + \frac{\partial f_{2g}}{\partial \gamma_g}\delta\gamma_g + \frac{\partial f_{2g}}{\partial \theta}\delta\theta + \frac{\partial f_{2g}}{\partial \eta}\delta\eta$$

$$+ \frac{\partial f_{2g}}{\partial T}\delta T + \frac{\partial f_{2g}}{\partial \delta f}\delta(\delta f) + \left\{\left(\frac{\partial f_{2g}}{\partial V_g} + \frac{2f_{2g}}{V_g}\right)\frac{\partial V_a}{\partial w}\right.$$

$$\left. + \left(\frac{\partial f_{2g}}{\partial \gamma_g} - f_{2g}\tan\gamma_g + \frac{f_{1g}}{V_g}\right)\frac{\partial \gamma_a}{\partial w}\right\} w \qquad (3.2.11)$$

$$\frac{d(\delta h)}{dx} = \sec^2\gamma_g\ \delta\gamma_g \qquad (3.2.12)$$

All the coefficients refer to nominal path.

It is necessary to evaluate $\partial V_a/\partial x$ and $\partial\gamma_a/\partial x$ as a function of V_g and γ_g (see Figure 3.1).

$$V_a = (V_g^2+w^2+2V_g w\cos\gamma_g)^{1/2} \qquad (3.2.13)$$

$$\frac{\partial V_a}{\partial w} = \frac{V_a - V_g}{w}\bigg|_{w\to 0} = \frac{V_g\left[1+\frac{2w}{V_g}\cos\gamma_g + \frac{w^2}{V_g^2}\right]^{1/2} - V_g}{w}\bigg|_{w\to 0}$$

$$= \frac{V_g}{w}\ \frac{w}{V_g}\cos\gamma_g = \cos\gamma_g \qquad (3.2.14)$$

also,

$$\gamma_a = \tan^{-1}\frac{V_g\sin\gamma_g}{V_g\cos\gamma_g + w} \qquad (3.2.15)$$

$$\frac{\partial\gamma_a}{\partial w}\bigg|_{w\to 0} = \lim_{w\to 0}\ \frac{-\dfrac{V_g\sin\gamma_g}{(V_g\cos\gamma_g+w)^2}}{1+\dfrac{(V_g\sin\gamma_g)^2}{(V_g\cos\gamma_g+w)^2}}$$

$$= - \frac{V_g \sin \gamma_g}{V_g^2 \cos^2 \gamma_g + V_g^2 \sin^2 \gamma_g}$$

$$= - \frac{\sin \gamma_g}{V_g} \qquad (3.2.16)$$

The subscript g is removed now with the understanding that all values refer to nominal ground values. Arranging it in the state space form,

$$\frac{dZ}{dx} = F(x)Z + G(x)U + \Gamma(x)w \qquad (3.2.17)$$

where,

$$Z = \begin{bmatrix} \delta V_g \\ \delta \gamma_g \\ \delta h \end{bmatrix} \qquad F(x) = \begin{bmatrix} \frac{\partial f_1}{\partial V} & \frac{\partial f_1}{\partial \gamma} & 0 \\ \frac{\partial f_2}{\partial V} & \frac{\partial f_2}{\partial \gamma} & 0 \\ 0 & \sec^2 \gamma & 0 \end{bmatrix} \triangleq \begin{bmatrix} f_{11} & f_{12} & 0 \\ f_{21} & f_{22} & 0 \\ 0 & \sec^2 \gamma & 0 \end{bmatrix}$$

$$G(x) = \begin{bmatrix} \frac{\partial f_1}{\partial \theta} & \frac{\partial f_1}{\partial \eta} & \frac{\partial f_1}{\partial T} & \frac{\partial f_1}{\partial \delta F} \\ \frac{\partial f_2}{\partial \theta} & \frac{\partial f_2}{\partial \eta} & \frac{\partial f_2}{\partial T} & \frac{\partial f_2}{\partial \delta F} \\ 0 & 0 & 0 & 0 \end{bmatrix}$$

$$\triangleq \begin{bmatrix} g_{1\theta} & g_{1\eta} & g_{1T} & g_{1\delta f} \\ g_{2\theta} & g_{2\eta} & g_{2T} & g_{2\delta f} \\ 0 & 0 & 0 & 0 \end{bmatrix}$$

$$U = \begin{bmatrix} \delta\theta \\ \delta\eta \\ \delta T \\ \delta(\delta f) \end{bmatrix}$$

$$\Gamma(x) = \begin{bmatrix} (f_{11}+f_1/V)\cos\gamma - \frac{\sin\gamma}{V}\left(f_{12}-f_1\tan\gamma-f_2V\right) \\ (f_{21}+2f_2/V)\cos\gamma - \frac{\sin\gamma}{V}\left(f_{22}-f_2\tan\gamma+\frac{f_1}{V}\right) \\ 0 \end{bmatrix} \qquad (3.2.18)$$

There are four control variables: Incremental pitch angle, $\delta\theta$ (changed by elevator deflection or rotor cyclic pitch control), incremental rotor shaft tilt, $\delta\eta$, incremental thrust, δT (varied using collective pitch control), and incremental flap deflection, $\delta(\delta f)$.

3.3 Quadratic Synthesis

For the system given by equation (3.2.17) we use the quadratic synthesis method to minimize

$$J = \frac{1}{2} Z^T(x_f) S_{x_f} Z(x_f)$$

$$+ \frac{1}{2} \int_{x_0}^{x_f} (Z^T(x) A(x) Z(x) + U^T(x) B(x) U(x)) dx$$

(3.3.1)

where A and B may be constant or functions of the independent variable. One possible choice of S_{x_f}, A and B is suggested by Bryson and Ho (BR-1). This choice uses a constant A and B and is good as a starting value in most cases. However, in this system this may not be true because of the change in configuration from helicopter to cruise mode and vice versa. In other words the system definition matrices, F, G and Γ vary with x considerably. The system is very sensitive to variations in η when the speed is low. If constant values are taken from matrices A and B, the gains tend to be undesirably high at low speeds.

While it is clear that it is desirable to use x-varying matrices A and B, the choice of x-dependence is not clear. One reasonable way, we think, would be to choose

$$A^{-1}(x) \sim \max Z(x) Z^T(x)$$

For this case these equations were found to be very useful in making an initial guess. To simplify things, we used B depending linearly on V.

The solution to the optimization problem (equations (3.2.17) and (3.3.1)) requires the solution to the well-known Riccati equation

$$\frac{dS}{dx} = -SF-F^TS-A+SGB^{-1}G^TS \qquad S(x_f) = S_{x_f} \tag{3.3.3}$$

The equation can be integrated backward starting from the known final condition. The control can, then, be found as a function of the state variables,

$$U = -B^{-1}G^TSZ = CZ \tag{3.3.4}$$

3.4 Control in the Presence of Wind

In the presence of wind, it is helpful to feed back an estimated value of the wind with a gain. To derive an equation for this gain, a model for the wind velocity is needed. A reasonable model is

$$\dot{w} = Ew + \text{white noise} \tag{3.4.1}$$

Adjoining this equation to the other state equations (3.2.17) we have:

$$\begin{bmatrix} \dot{Z} \\ \dot{w} \end{bmatrix} = \left[\begin{array}{c:c} F & \Gamma \\ \hdashline 0 & E \end{array}\right] \begin{bmatrix} Z \\ w \end{bmatrix} + \begin{bmatrix} G \\ 0 \end{bmatrix} U$$

or,

$$\dot{Z}_w = F_w Z_w + G_w U \qquad (3.4.2)$$

It can be shown (BR-2) that the gains on δV, $\delta\gamma$, δy are the same as when w = 0, and that the gains on the estimated wind w are obtained by solving the following differential equation for R

$$\dot{R} = -S\Gamma - RE - F^T R + SGB^{-1}G^T R \qquad R(x_f) = 0 \qquad (3.4.3)$$

where,

$$R(x) = \begin{Bmatrix} R_1 \\ R_2 \\ R_3 \end{Bmatrix} \quad \text{and} \quad C_w = -B^{-1}G^T R \qquad (3.4.4)$$

For a constant wind $E \triangleq 0$.

3.5 Estimation of the Wind Velocity

To control the aircraft effectively in the presence of wind, it is necessary to obtain an estimate of the wind velocity. It could be found by direct measurement or from some other external source. However, if this is not possible, the wind velocity may be estimated using measurements of aircraft motion. This method of estimation is described here.

The state equations and the equation governing the average wind velocity are

$$\dot{Z} = F(x)Z + G(x)U + \Gamma(x)w \qquad (3.2.17)$$

$$\dot{w} = Ew \qquad (3.4.1)$$

Take $\dot{Z}$ as the measurement (assuming Z is available). Then the estimated value, $\hat{w}$, of w can be obtained by

$$\dot{\hat{w}} = E\hat{w} + K(x)[\dot{Z}-\dot{\hat{Z}}] \qquad (3.5.1)$$

From equation (3.2.17),

$$\dot{\hat{Z}} = FZ + GU + \Gamma\hat{w} \qquad (3.5.2)$$

Substituting equations (3.2.17) and (3.5.2) in equation (3.5.1) we have,

$$\dot{\hat{w}} = E\,\hat{w} + K(x)\Gamma(x)[w-\hat{w}] \qquad (3.5.3)$$

Subtracting equation (3.4.1) from equation (3.5.3)

$$\frac{d}{dx}(w-\hat{w}) = E(w-\hat{w}) - K(x)\Gamma(x)(w-\hat{w}) \qquad (3.5.4)$$

Defining the error e as,

$$e = w-\hat{w} \qquad (3.5.5)$$

$$\frac{de}{dx} = \left\{E-K(x)\Gamma(x)\right\} e \qquad (3.5.6)$$

By a suitable choice of the x-varying gain K(x) the characteristic root of (3.4.6) can be placed anywhere one

TWO IMPLEMENTATIONS ARE POSSIBLE

(i) if $\dot{Z}$ is available

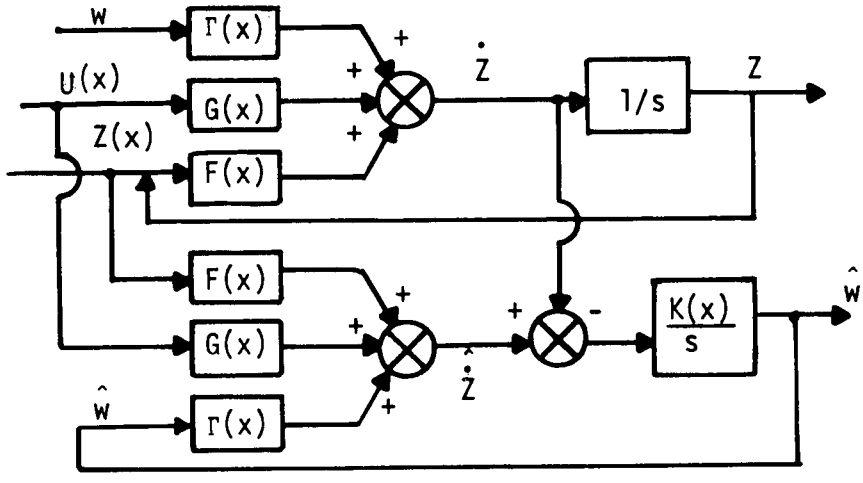

(ii) if $\dot{Z}$ is not available

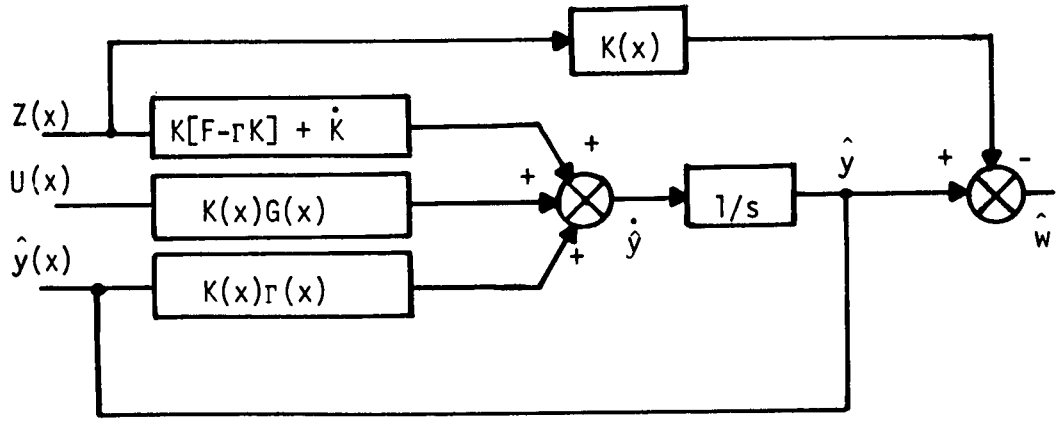

Figure 3.2 Estimation of Wind Velocity

desires, for all x.

Equation (3.5.3) can be put in another form using only Z and not $\dot{Z}$:

$$\dot{\hat{w}} - \dot{K}Z - K\dot{Z} = E\hat{w} + K\Gamma w - K\Gamma\hat{w} - \dot{K}Z - K[FZ + GU + \Gamma w]$$

i.e.,

$$\frac{d}{dx}(\hat{w} - KZ) = (E - K\Gamma)\{\hat{w} - KZ\} - KGU - \{KR + \dot{K} - (E - K\Gamma)K\}Z \tag{3.5.7}$$

defining

$$\hat{y} = \hat{w} - KZ,$$

$$\frac{d}{dx}\hat{y} = (E - K\Gamma)\hat{y} - KGU - (K\Gamma + \dot{K} - (E - K\Gamma)K)Z \tag{3.5.8}$$

This is another way the observer can be implemented. The gain K(x) can be chosen as before. The block diagram for two possible observers is shown in Figure 3.2.

3.6 RMS Response in Presence of Fluctuating Wind

A tilt-rotor aircraft may encounter fluctuating wind velocity along its flight path because of variation in wind velocity with (a) distance, and (b) time. When the correlation distance is small, it is not possible to estimate the wind velocity accurately. If the correlation distance is infinitesimally small, i.e., the wind is "white", the gains on the estimated wind do not change the response since it is impossible to predict the future behavior of the wind from past information. Substituting for U from equation (3.3.4) in equation (3.2.17), we have

$$\frac{dZ}{dx} = (F+GC)Z+\Gamma w \ . \qquad (3.6.1)$$

If w is assumed white, with time correlation

$$E[w(t)w(\tau)] = Q(t)\delta(t-\tau) \qquad (3.6.2)$$

$$\bar{Z}(x) = E(Z(x)Z^T(x)) \qquad (3.6.3)$$

it can be shown that (BR-1),

$$\frac{d\bar{Z}}{dx} = (F+GC)\bar{Z} + \bar{Z}(F+GC)^T + \Gamma Q(x)\Gamma^T \qquad (3.6.4)$$

where,

$$E(w(x)w(x')) = Q(x)\delta(x-x') \qquad (3.6.5)$$

Since,

$$\frac{dt}{dx} = \frac{1}{V \cos \gamma}$$

equation (3.6.1) can also be written as

$$\frac{dZ}{dt} = (F+GC)Z \ V \cos \gamma + \Gamma w \ V \cos \gamma \qquad (3.6.6)$$

Hence

$$\frac{d\bar{Z}}{dt} = (F+GC)V \cos \gamma \bar{Z}+\bar{Z} \ V \cos \gamma(F+GC)^T+\Gamma Q(t)\Gamma^T V^2 \cos^2 \gamma \qquad (3.6.7)$$

Changing back to x as the independent variable,

$$\frac{d\bar{Z}}{dx} = (F+GC)\bar{Z}+\bar{Z}(F+GC)^T+\Gamma \ Q(t)V \cos \gamma \ \Gamma^T \qquad (3.6.8)$$

Comparing (3.6.4) and (3.6.8), we have

$$Q(x) = Q(t)V \cos \gamma \tag{3.6.9}$$

Equation (3.6.9) is a general equation for changing the independent variable. Equation (3.6.4) can be solved using equation (3.6.9) and the initial condition,

$$\bar{Z}(x_0) = E\left\{Z(x_0)Z^T(x_0)\right\} \tag{3.6.10}$$

3.7 Summary

This chapter presented a general perturbation guidance technique for a tilting proprotor aircraft. This scheme can be simplified in most cases. For instance, it may not be necessary to use all four control variables or it may be unnecessary to feed back all state variables to all controls. The next two chapters consider take-off and landing trajectories for the Bell Model 266 and show how simplications can be made in those cases.

CHAPTER IV

Longitudinal Guidance During Take-off

4.1 Introduction

The general method for VTOL aircraft guidance, presented in the last chapter is modified and simplified to develop a guidance scheme for the take-off phase of the flight. The take-off involves transition from a low-speed helicopter mode to a high-speed cruise mode, in which the rotors are used as propellers. The techniques applied here can be used for any take-off trajectory. However, a particular flight path has been chosen for illustration.

The selected flight path is shown in Figures 4.1a and 4.1b. The aircraft starts vertically from zero speed.

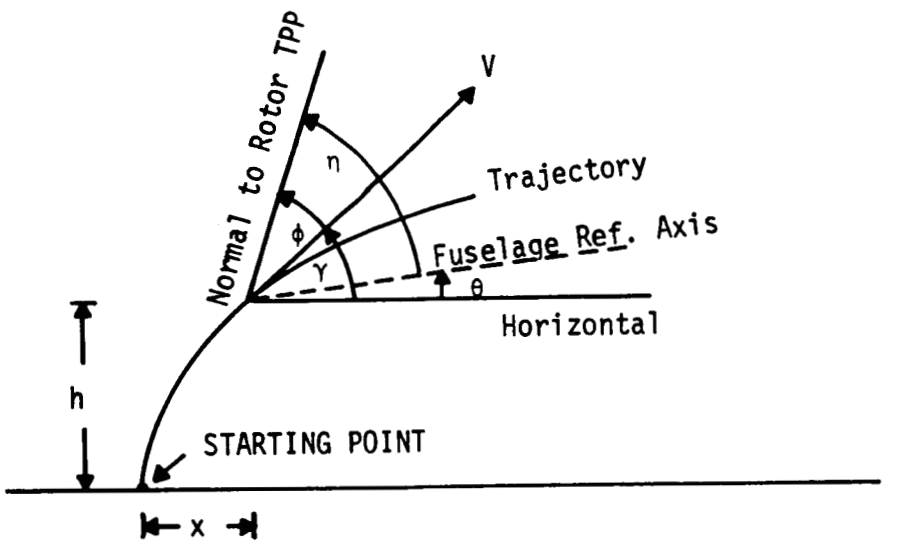

Figure 4.1b Terminology Used for Take-Off Trajectory

The flight path angle is maintained at $\pi/2$ until a speed of 2.85 m sec^{-1} is reached. Then the aircraft starts the

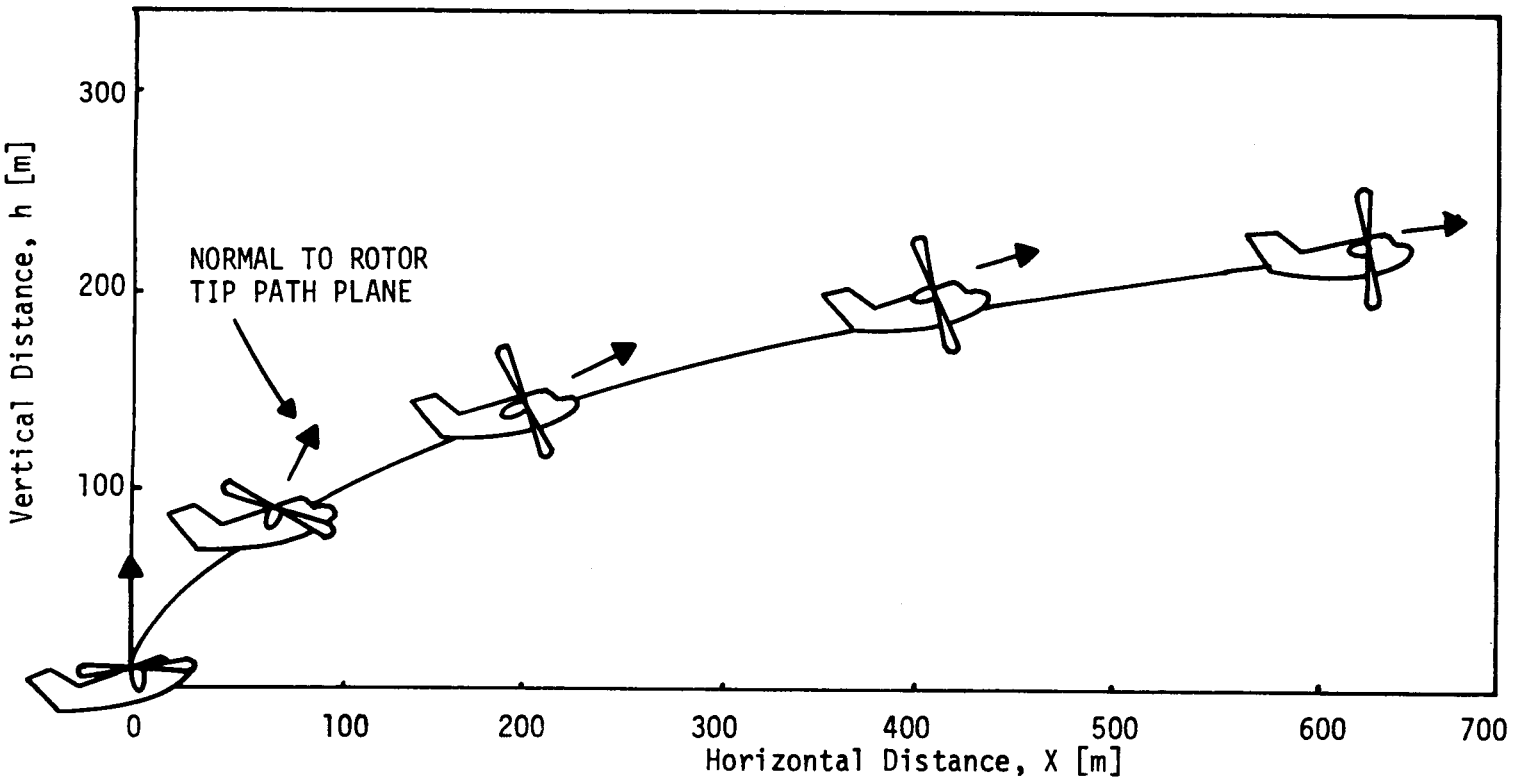

Figure 4.1a Nominal Take-off Trajectory

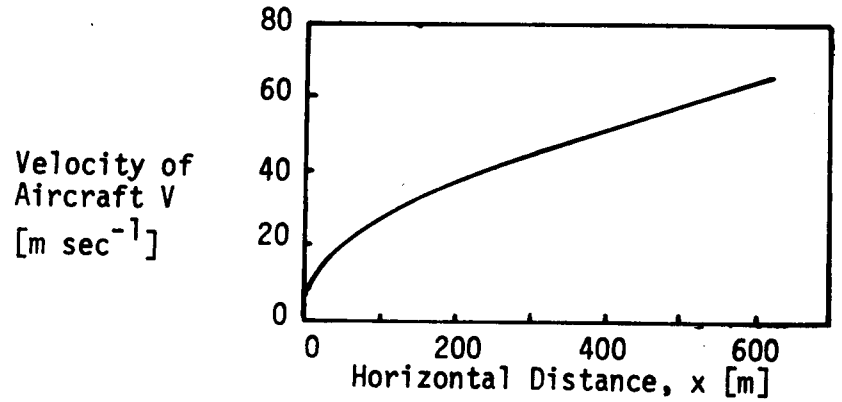

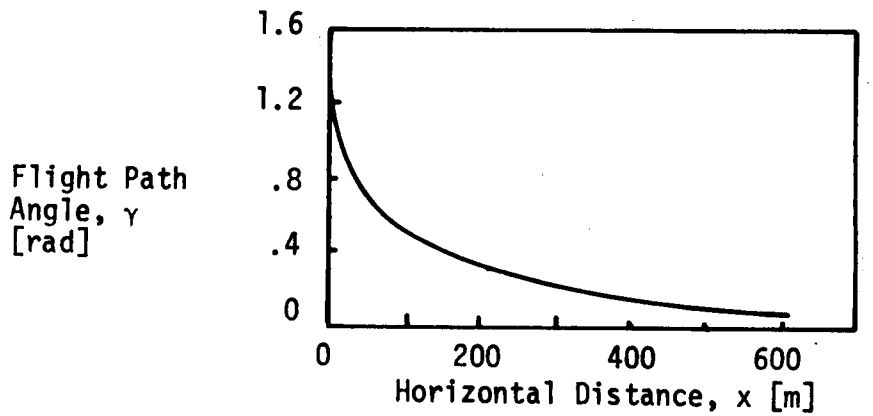

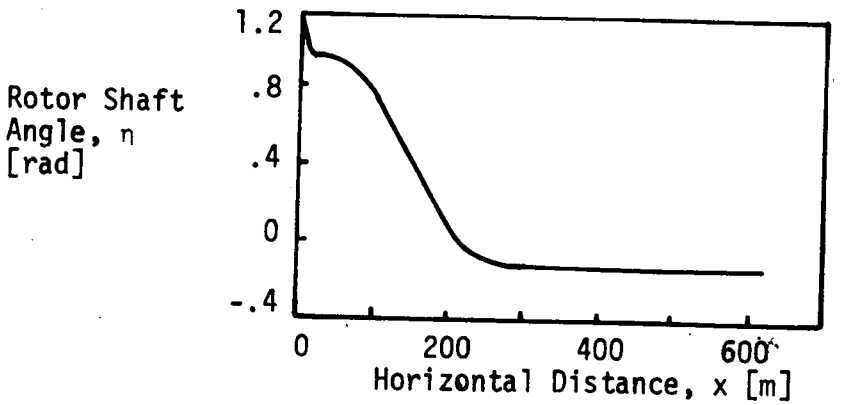

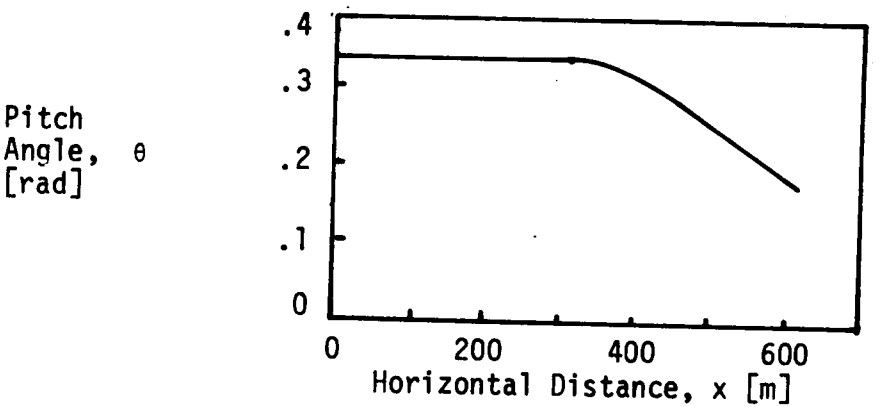

Figure 4.2 V,γ,θ,η as a Function of x for Nominal Trajectory

transition at a constant normal acceleration of -1.6 m sec^{-1}. The thrust is fixed at its maximum available value at all times. The flaps and aileron-flaps are deflected as much as possible (57 degrees) before starting, to reduce download on the wings, and are retracted as the aircraft gains speed. The pitch angle is chosen so that the wings are loaded as much as possible with a 20% margin for stall. We specify maximum and minimum allowable values of the pitch angle. Figure 4.2 shows nominal values of flight path angle, velocity, pitch angle and rotor shaft deflection angle.

4.2 Simplifying the Model

The problem of guidance during take-off has control variable constraints. The thrust is fixed at the maximum value; hence positive values of δT are not feasible. There are similar constraints on flap deflection and pitch angle during a portion of the take-off trajectory. One way to use quadratic synthesis is to use less (more) than the maximum (minimum) values of these control variables during the nominal flight leaving a certain margin for feedback control. However, in this case, there are four control variables and it is not necessary to use all of them to achieve the desired goal. We decided to use thrust and flap deflection as open-loop controls and rotor shaft tilt and pitch angles as feedback controls. The installed power and rotor size in a tilt-rotor VTOL aircraft are dictated by the take-off requirements; hence using anything but the maximum thrust during take-off is economically undesirable. The flap deflection is not a very effective control variable. The linearized equations in the presence of wind (equations (3.4.2)) simplify to

$$\frac{dZ_w}{dx} = F_w(x)Z_w + G_{TO}(x)\, u_{TO} \qquad (4.2.1)$$

where F_w, Z_w, Γ and w are defined in equations (3.2.18) and (3.4.2) and G_{TO} and u_{TO} are

$$G_{TO} = \begin{bmatrix} g_{1\eta} & g_{1\theta} \\ g_{2\eta} & g_{2\theta} \\ 0 & 0 \\ 0 & 0 \end{bmatrix}$$

$$u_{TO} = \begin{bmatrix} \delta\eta \\ \delta\theta \end{bmatrix} \qquad (4.2.2)$$

The drag on the rotors and the nacelles is small along most of the flight path and is dropped.

4.3 Choice of Weighting Matrices

Tentative specifications for matrices A, B, and S_{x_f} in equation (3.3.1) were made using equations (3.3.2) and (3.3.3) as guidelines. A simplified linear V-dependence is used. Final values of these matrices were obtained by cut and try. They are*

$$A = \begin{bmatrix} .00021 & 0 & 0 & 0 \\ 0 & .04 & 0 & 0 \\ 0 & 0 & .00044\cos^2\gamma & 0 \\ 0 & 0 & 0 & 0 \end{bmatrix}$$

*Units in meters, sec, rad.

$$B^{-1} = \begin{bmatrix} .14\ V & \\ 0 & \begin{cases} .3 & V>24.5 \text{ m sec}^{-1} \\ 0 & V<24.5 \text{ m sec}^{-1} \end{cases} \end{bmatrix}$$

$$S_f = \begin{bmatrix} .069 & 1.2 & .02 & -.0026 \\ 1.2 & 170.0 & 2.9 & 1.1 \\ .02 & 2.9 & .063 & .013 \\ -.0026 & 1.1 & .013 & .048 \end{bmatrix}$$

(4.3.1)

The A_{33} term in matrix A varies as $\cos^2\gamma$ because we are interested in minimizing the square of the distance normal to the flight path while the state variable Zw_3 is the vertical distance. It is clear from Section 3.4 and the fact that the wind velocity w, is uncontrollable, that the weight A_{44} makes no difference. At low speeds, the angle of attack of the wing, and hence the pitch angle, does not affect the forces very much. Below a speed of 24.5 m sec^{-1}, we put $(B^{-1})_{22}$ equal to zero to reflect this. The matrix S_f is chosen as the steady state Riccati gain matrix for a constant coefficient system with state and weighting matices corresponding to the terminal time.* This ensures that no gain is abnormal near the terminal condition. In cases where the process continues beyond the terminal design time, we consider this a useful algorithm for picking the Riccati gain matrix at the terminal point.

*In this case S_{x_f} is computed using w = -.0001w+"white"noise to avoid the problem of zero eigenvalue in the eigenvector decomposition technique.

4.4 Control Gains and Aircraft Performance in the Presence of Wind

The gains on rotor shaft tilt and pitch angle are shown as a function of the horizontal distance x in Figures 4.3 and 4.4. These gains are for aircraft speeds greater than 2.85 m sec^{-1}. During the vertical flight immediately after take-off, the horizontal distance does not change and it cannot be used as the independent variable. This problem is discussed later in Section 4.5.

All gains are negative or zero throughout the flight path. The gains on pitch angle are zero for $x < 64$ m since we put $(B^{-1})_{22}$ equal to zero for x in this range. Notice that most of these gain programs can be approximated by combinations of constant values and ramp functions.

Controlled tilt-rotor aircraft flight paths in the presence of wind or initial disturbances were computed using the nonlinear equations. At any point along the flight path, incremental pitch angle and rotor shaft tilt are computed using deviations in aircraft velocity, flight path angle, vertical distance from the nominal trajectory, and estimated wind velocity. A continuous implementation is assumed.

Figure 4.5 shows the flight path for the tilt-rotor VTOL aircraft with initial errors in flight path angle (-5.7°) and distance away from the nominal trajectory (vertical distance = -5m). The errors die out quite quickly. The normal distance of this trajectory from the nominal one is almost zero at the final horizontal position. With no control there will be a terminal error of 10 m. The figure also shows variations of $\delta\theta$ and $\delta\eta$. By the time the pitch angle control comes into action the errors are already small. The maximum value of $\delta\eta$ is less than 6° and $\delta\theta$ is

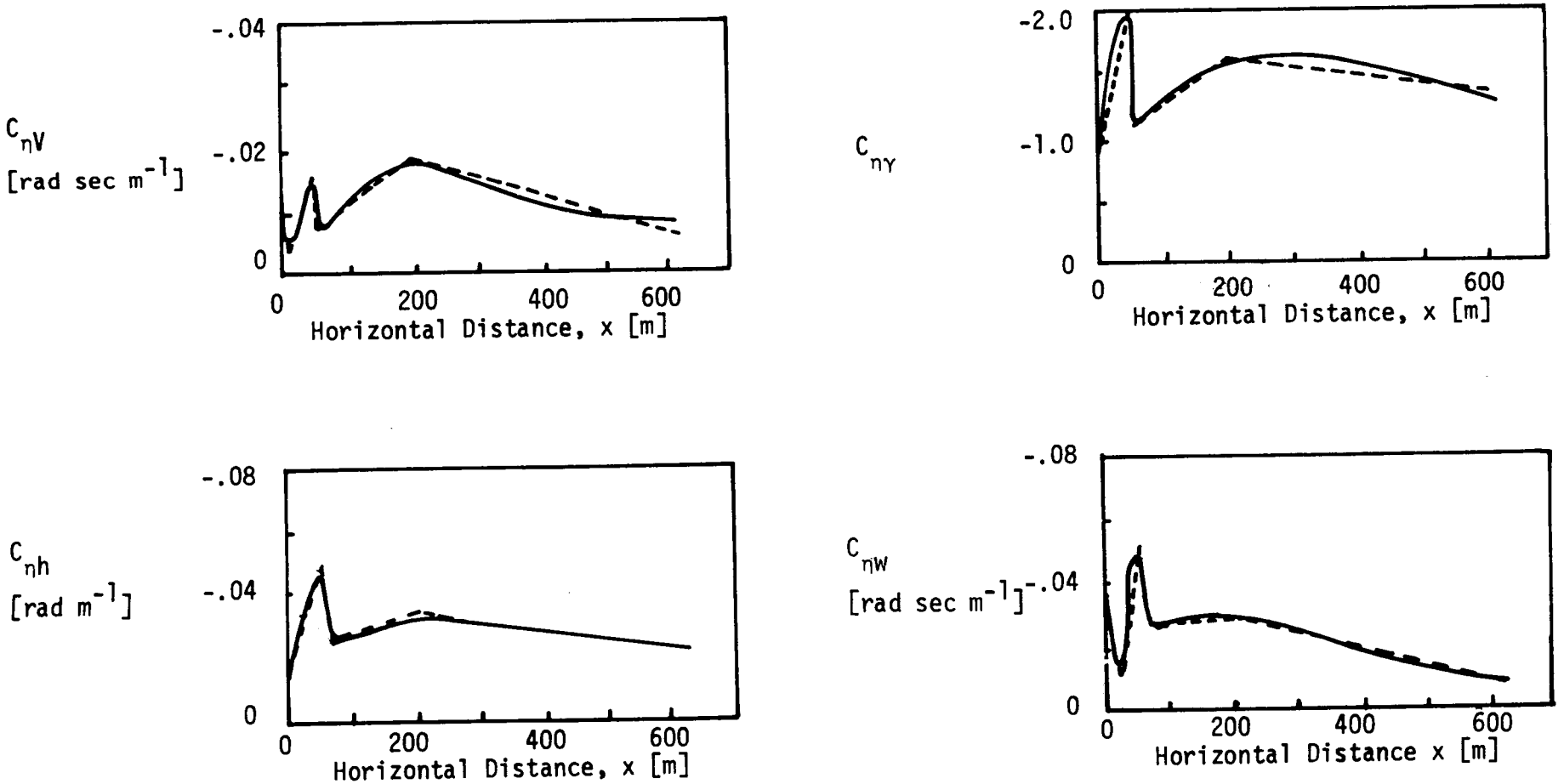

Figure 4.3 Gains on Rotor Shaft Tilt

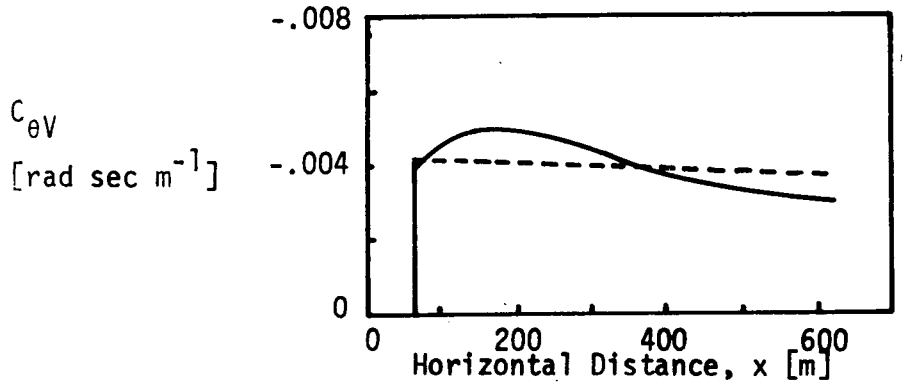

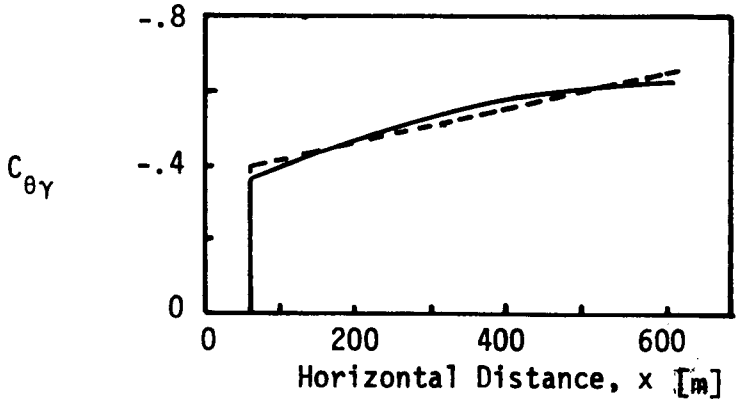

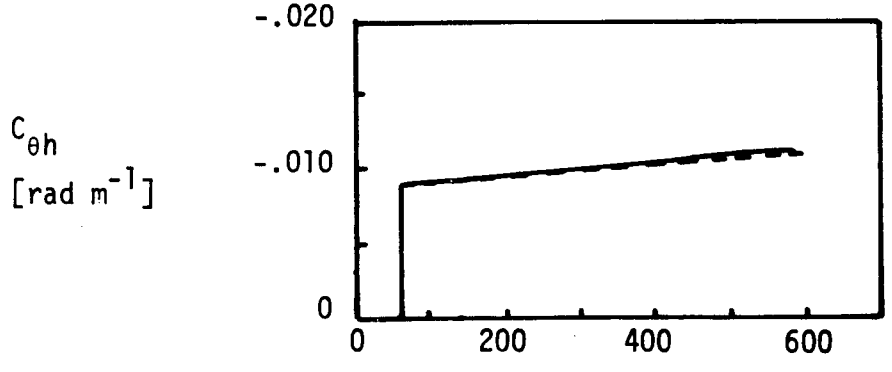

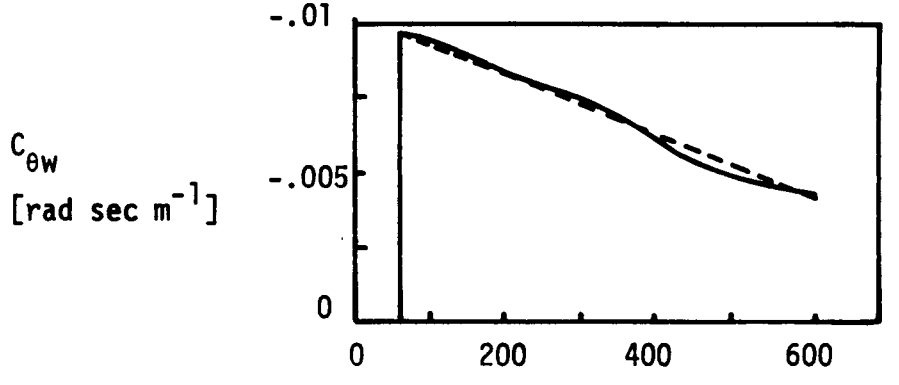

Figure 4.4 Gains on Pitch Angle

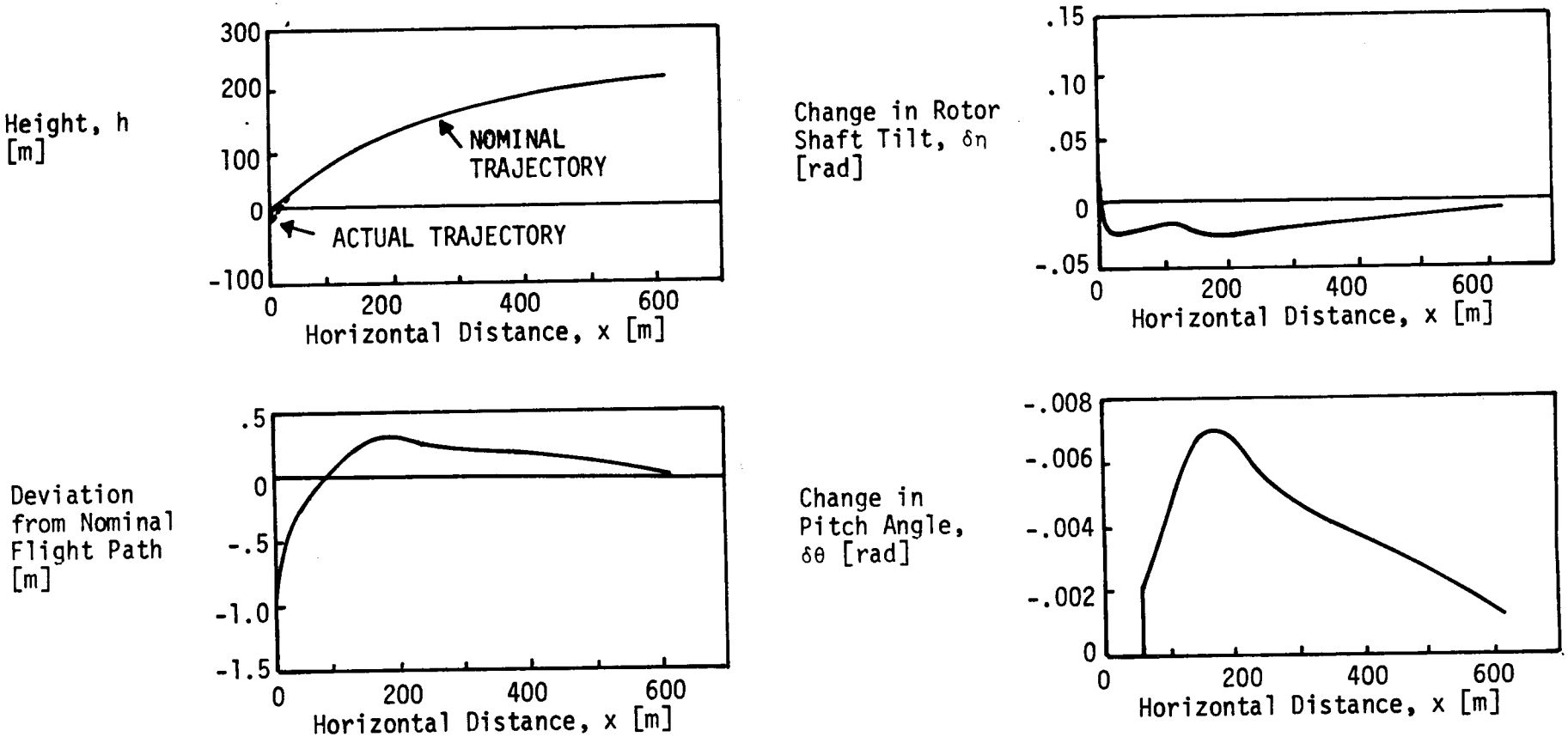

Figure 4.5 Trajectory and Control Effort with Initial Disturbance
[e_h = -5.0 m, e_γ = -.1 rad]

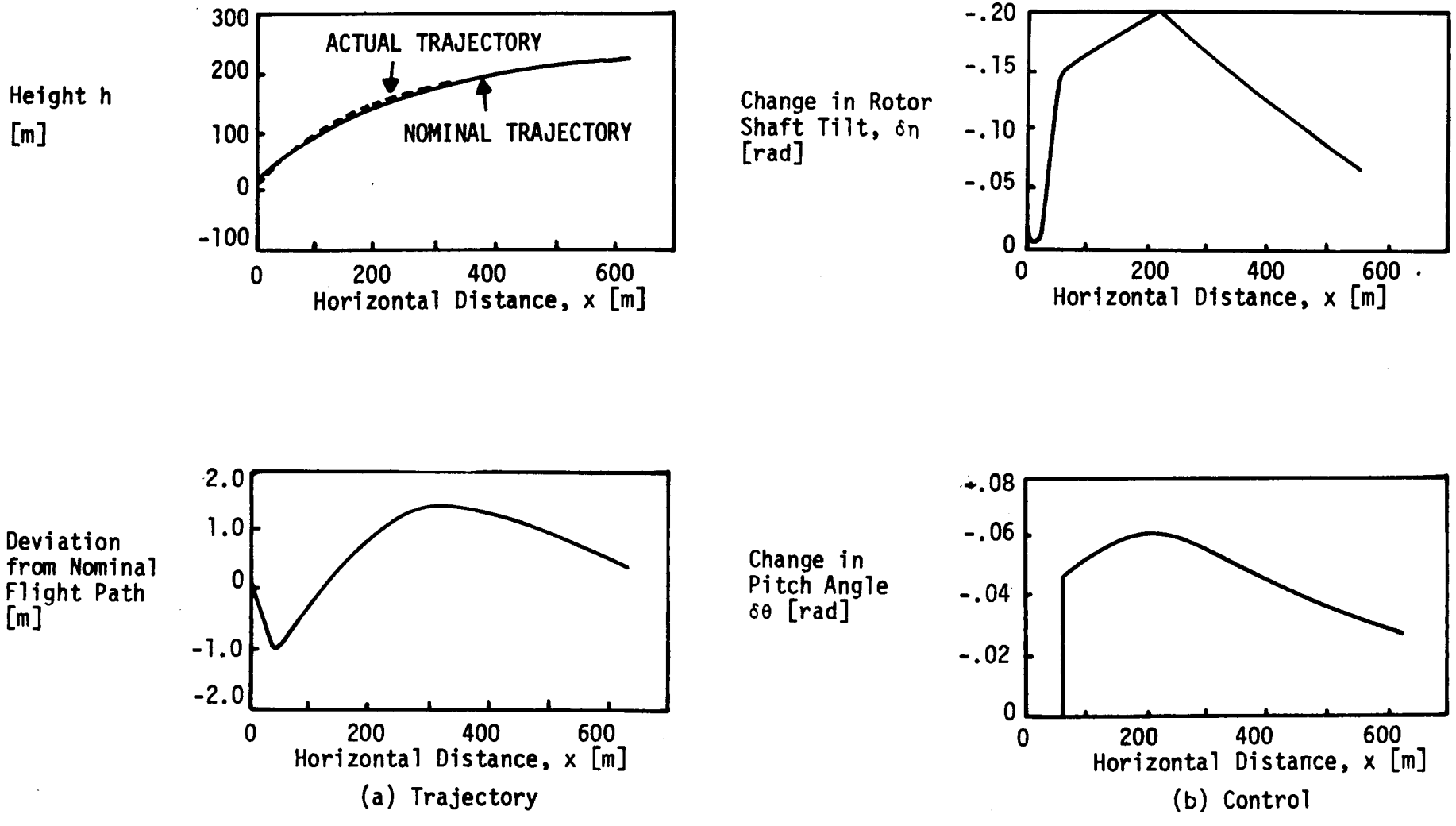

Figure 4.6 Trajectory and Control Effort in the Presence of 5 m sec^{-1} Head Wind [Wind Velocity Estimated].

always small.

A trajectory in the presence of a steady head wind of 5.0 m sec^{-1} is shown in Figure 4.6. Initially this trajectory falls below the nominal trajectory. The error in position starts from a low value, reaches a maximum value of 1.4 m at horizontal distance 300 m and then decreases again. The final error is less than .4 m. In the absence of feedback control it would be 35 m. The deviations in rotor shaft tilt angle and pitch angle reach their maximum values at 200 m. By this point the wind velocity is estimated within 5% and there is enough $\delta\theta$ and $\delta\eta$ to counterbalance the effect of wind as much as possible. This required amount of $\delta\theta$ and $\delta\eta$ decreases with increasing speed.

Using control gains computed above many other flight paths were computed. The flight paths obtained by assuming perfect knowledge of wind were superior to the ones with a wind estimator. Feeding back estimated or otherwise measured wind velocity provides a considerable improvement.

Using the linearized system of equations, the root mean square (RMS) response is computed in the presence of random wind. Figures 4.7 and 4.8 show RMS values of state and control variables in the presence of a random wind with RMS value of 3.0 m sec^{-1} and correlation time of .30 sec (modelled "white"). All state variables are assumed to be known exactly. The RMS values of initial errors in velocity, flight path angle and height were taken as 1.0 m sec^{-1}, .01 rad, and 3.0 m respectively.

Figures 4.9 and 4.10 show RMS values of state and control variables in the presence of wind consisting of two components, (a) a random wind as in the last case, and (b) a steady wind with RMS value 3.0 m sec^{-1}. The initial RMS errors are the same as in the last case. Initially the

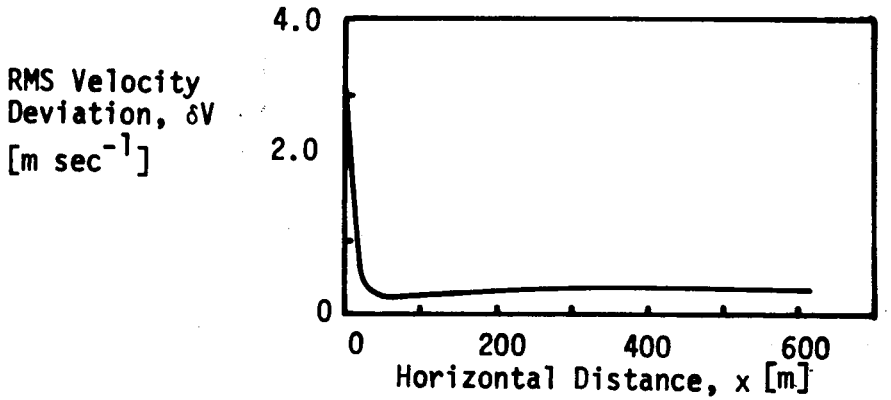

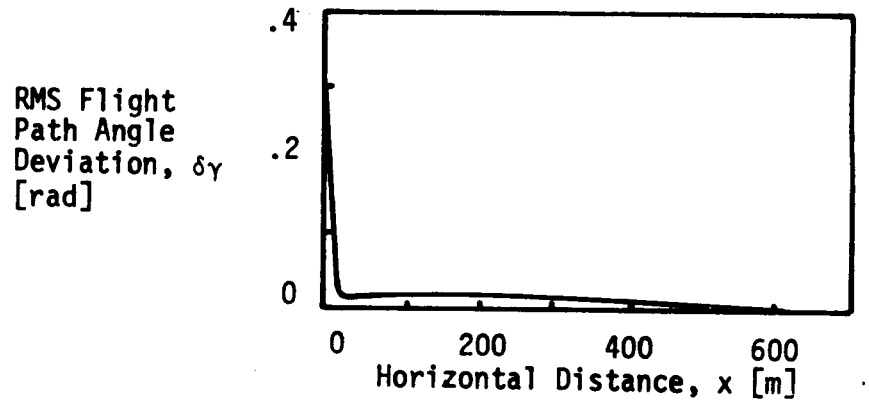

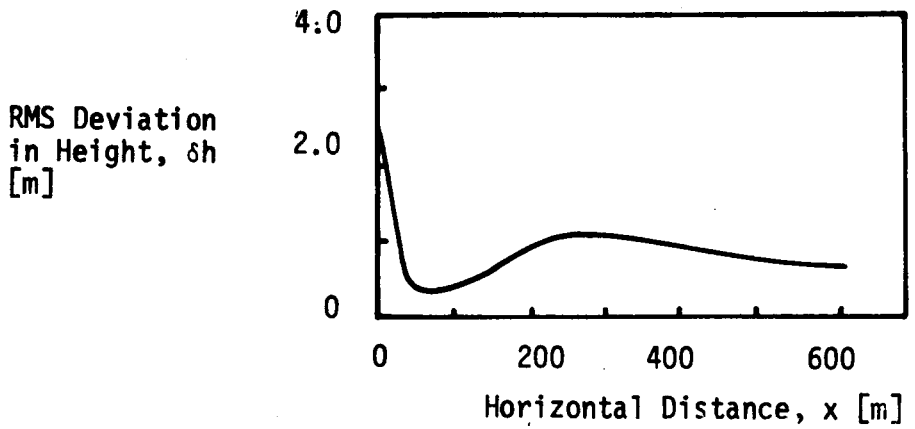

Figure 4.7 RMS State in the Presence of Random Wind ["white" with Power Spectral Density 5.4 $m^2 sec^{-1}$]

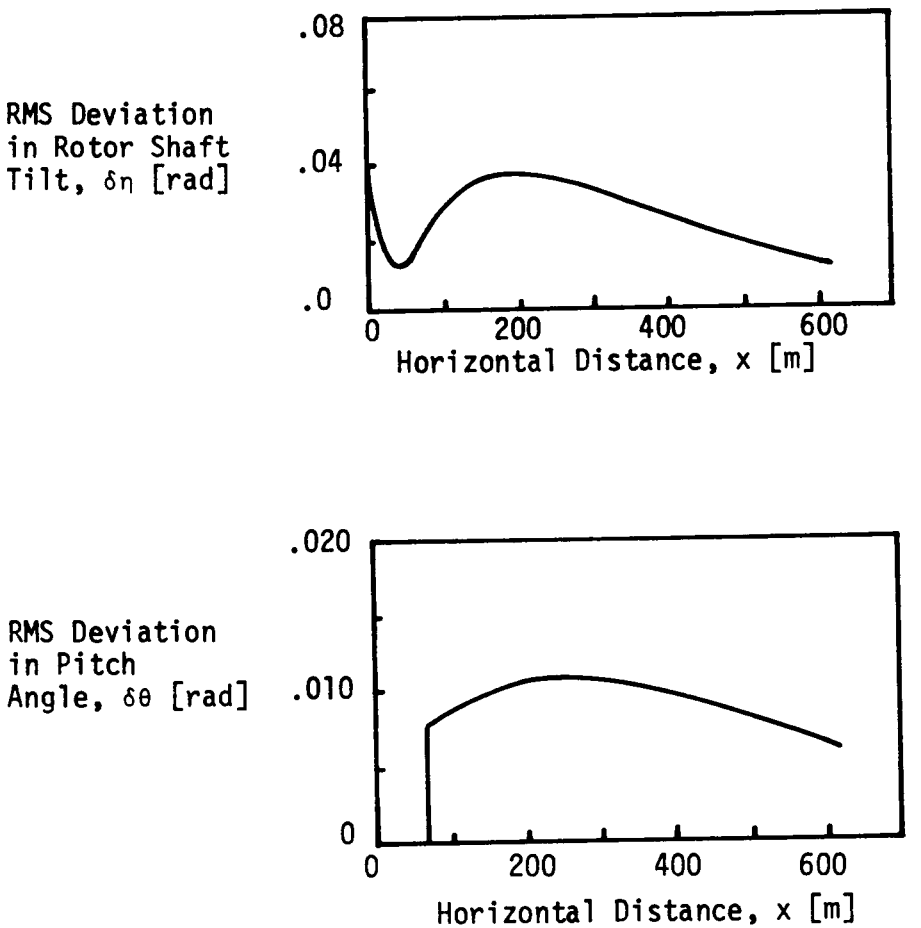

Figure 4.8 RMS Control in the Presence of Random Wind ["white" with Power Spectral Density 5.4 $m^2 sec^{-1}$]

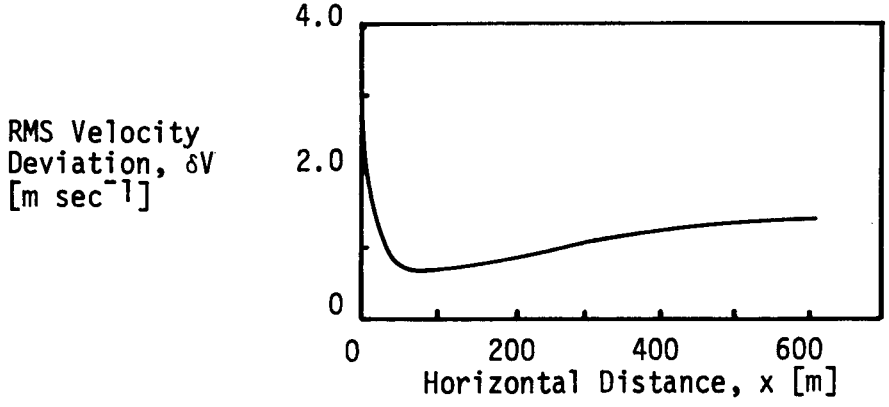

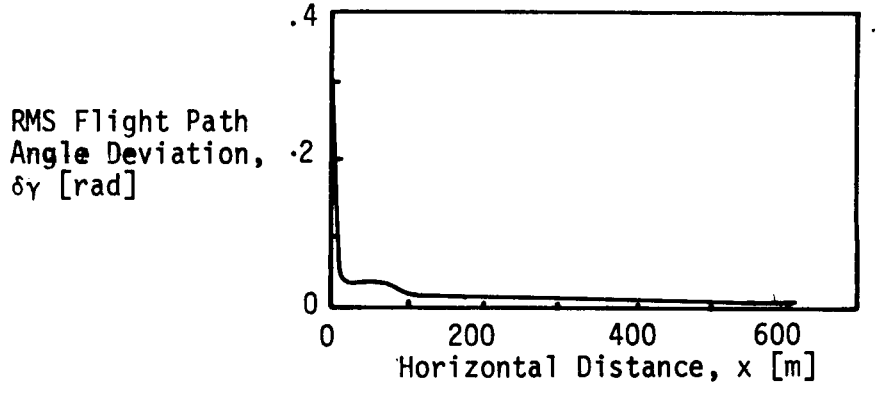

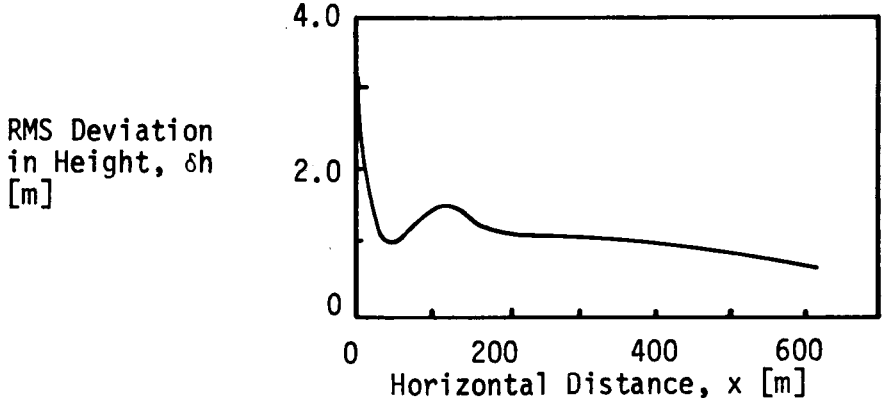

Figure 4.9 RMS State in the Presence of Random Wind
[$w=w_1+w_2$, w_1=random bias (RMS 3 m sec^{-1}),
w_2=white noise, power spectral density=5.4 $m^2 sec^{-1}$]

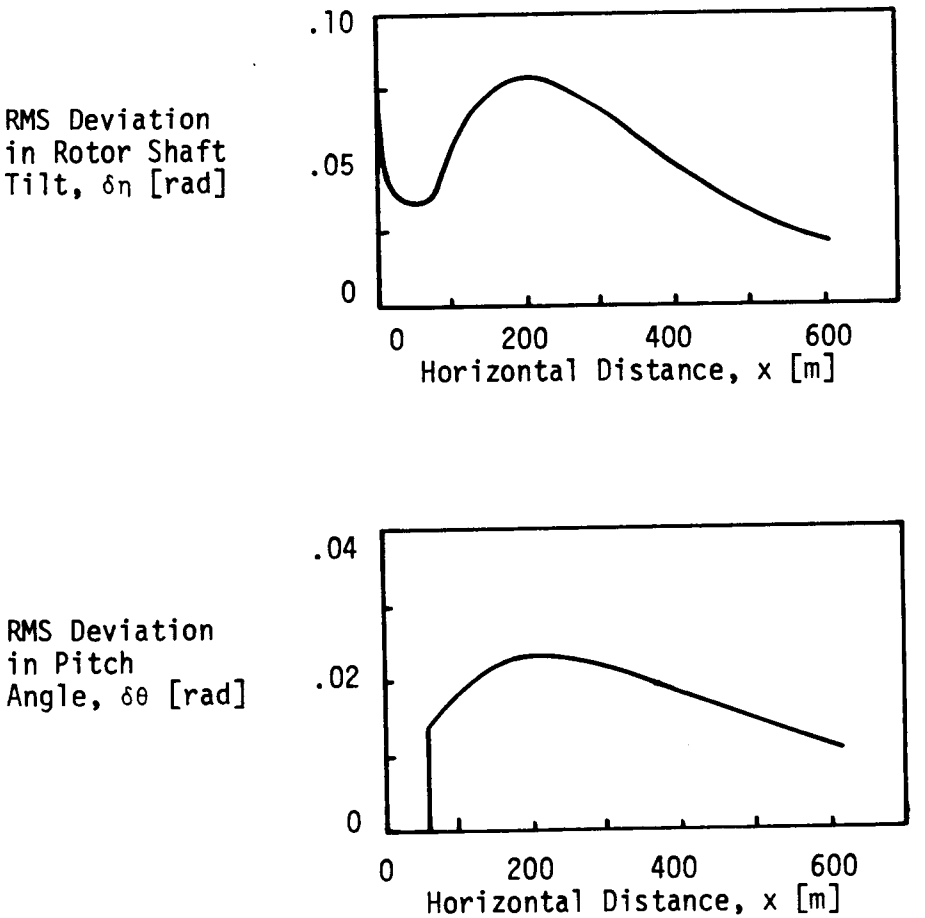

Figure 4.10 RMS Control in the Presence of Random Wind of Figure 4.9

errors increase and then they decrease. Within 100 m from the starting position the RMS errors reach almost a constant value. The RMS error in velocity is about 1.0 m sec^{-1} and in height is about 1.0 m. These errors are more than the corresponding errors in the last case where there is no steady wind. The RMS $\delta\eta$, the change in rotor shaft tilt angle, is always less than 6° and the RMS $\delta\theta$ never exceeds 1.5°. Less control is required in the absence of this steady wind. The errors in state variables and the required amount of control look quite reasonable.

4.5 Guidance at Low Speed

Immediately at take-off the flight path is vertical and horizontal distance is not a useful independent variable. Furthermore the assumption concerning the decoupling of the longitudinal and lateral vehicle motions is not very good.

One way to deal with these complications is to use a modified hover autopilot until the aircraft reaches a certain speed. Since commercial VTOL aircraft will probably have an autopilot hover mode, it should be easy to modify this mode so that it can be used at low speeds also. Hover autopilots for VTOL aircraft have been designed for example by Bryson and Hall (BR-2).

Even if the assumption of decoupling is considered satisfactory for this purpose there is another problem. At low speeds even when the flight path is not exactly vertical the gains and nominal values of state and control variables change rapidly as a function of the horizontal distance, x. Errors in estimation of x could cause some trouble. Under these circumstances it is better to use the height h as the independent variable during the initial part of the trajectory.

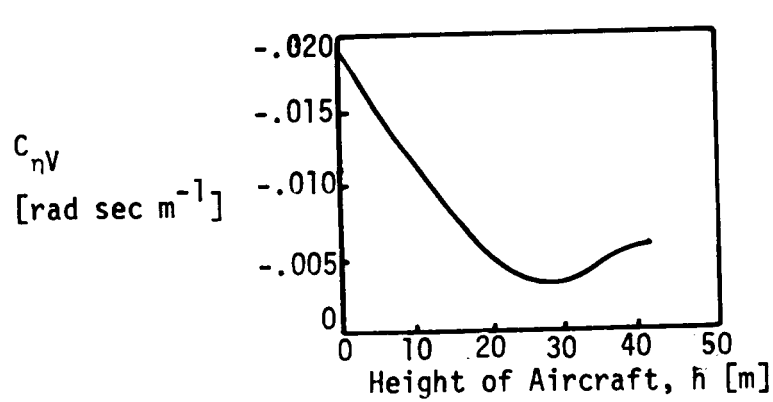

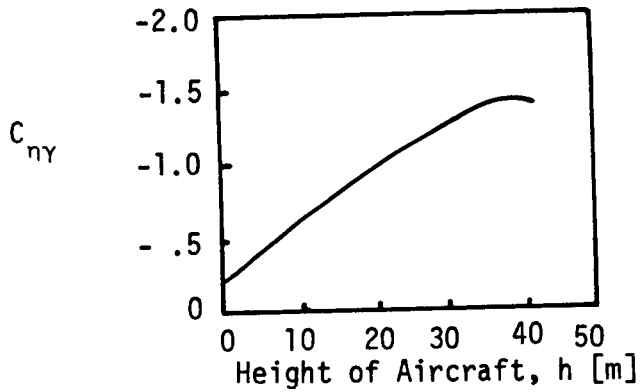

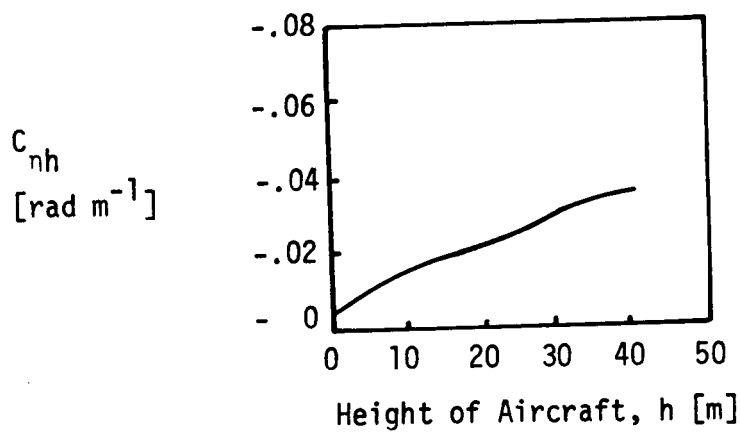

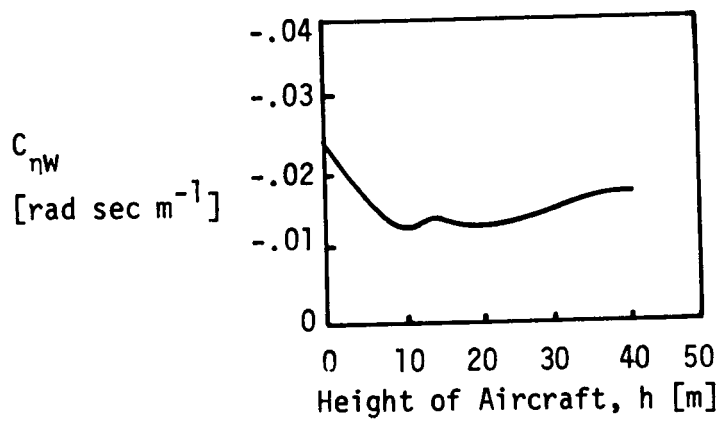

Figure 4.11 Gains on Rotor Shaft Tilt with Height as the Independent Variable

To do this it is necessary to relinearize the equations of motion.

Altitude, h, is used as the independent variable until the flight path angle is 45° and thereafter it is changed to x. The flight path angle is 45° at horizontal distance 27 m and height 41.7 m. The gains are shown in Figure 4.11 for $0 \leq h \leq 41.7$ m. In these computations the weighting matrices were not modified to account for a change in the independent variable. The gains do not change as rapidly as they did before.

4.6 Summary

Table IV-1 shows the control system performance with initial disturbances. The initial disturbance is -5.0 m in height and -.1 rad in flight path angle. The control system cuts down the error by a factor of about 100 while using a nominal amount of control.

Table IV-2 compares the control system under different conditions for a 5.0 m sec^{-1} steady head wind. In the absence of control, the average error (deviation normal to the nominal trajectory) is 24 m and the error at the beginning of cruise is 35 m. If the wind velocity is not estimated or measured the average error is 5.0 m and the error at the beginning of cruise is 2.6 m with the control system. The change in rotor shaft tilt angle averages 6.7° and reaches a maximum value of 11°. If the wind velocity is estimated the average error is 0.8 m and the error at the beginning of cruise is .4 m. The change in rotor shaft tilt angle still averages 6.7° and has a maximum of 11°. The performance is best when wind velocity is exactly known followed by the case where it is estimated.

CONTROL SYSTEM	DEVIATION NORMAL TO THE NOMINAL TRAJECTORY		CONTROL ACTION ON ROTOR SHAFT TILT ANGLE		CONTROL ACTION ON PITCH ANGLE	
	Ave Value*	Terminal Value	Max Value	Ave Value*	Max Value	Ave Value*
Exact gains	.14 m	.02 m	5.8°	.66°	.4°	.19°
Approx gains	.20 m	.015 m	5.7°	.79°	.45°	.22°
No control	9.5 m	10 m	-	-	-	-

* Average over horizontal distance x

Table IV-1 System Performance in the Presence of Initial Disturbances [e_h =-5.0 m, e_γ = -.1 rad]

Gains Approx	Exact Wind Vel	Wind Vel "Observer"	Deviation Normal to the Nominal Trajectory		Control Action on Rotor Shaft Tilt Angle		Control Action on Pitch Angle	
			Ave† Value	Terminal Value	Max Value	Ave† Value	Max Value	Ave† Value
No	No	No	5.0 m	2.6 m	11°*	6.6°	3.4°	2.3°
No	Yes	No	.70 m	.25m	11°	6.0°	3.0°	2.0°
No	No	Yes	.80 m	.35m	11°*	6.7°	3.5°	2.4°
Yes	No	No	5.2 m	2.7 m	11°	6.7°	3.5°	2.3°
Yes	Yes	No	.81 m	.20m	11°	6.0°	3.1°	2.1°
Yes	No	Yes	.82 m	.35m	11°*	6.7°	3.5°	2.4°
NO CONTROL			24 m	35 m	-	-	-	-

* There was a constraint imposed on the maximum values of $\delta\eta$ and $\delta\theta$ in the nonlinear equation. This is the maximum value

† Average over horizontal distance x

Table IV-2 Comparison of Different Control Laws in the Presence of 5.0 m sec^{-1} Head Wind

The x-varying control gains were approximated using a combination of constant values and ramp functions. The approximated gains are shown with dotted lines in Figures 4.3 and 4.4. This approximation reduces the storage requirement and computation time for an airborne computer considerably. Referring to Tables IV-1 and IV-2, we see that the approximate gains deteriorate the performance slightly. The approximated gains should be used in actual implementation.

CHAPTER V

Longitudinal Guidance During Landing

5.1 Introduction

This chapter deals with the control gains and the guidance scheme for a tilting proprotor VTOL aircraft during approach and landing. The technique is similar to the take-off case.

The nominal trajectory considered here is a straight line with a flight path angle of -5.7°. The initial aircraft velocity is 66.8 m sec^{-1} and the initial flap deflection is 14 degrees. To start with the rotors are unloaded and rotated at a rate of 5.7° sec^{-1} until the rotor shaft angle reaches 101 degrees. The flaps and the aileron-flaps are also turned at 5.7° sec^{-1} rate until they are deflected 57 degrees. The rotors start producing thrust when the rotor shaft angle exceeds 90° so that a component of the thrust decelerates the aircraft. The pitch angle is fixed at -6° during powered flight.* The aircraft trajectory is shown in Figure 5.1. Nominal values of velocity, thrust, pitch angle and rotor shaft deflection angle are shown in Figure 5.2.

5.2 Simplifying the Model

The linearized equations of Chapter III have been simplified as in the case of take-off guidance with one exception. During take-off the rotor thrust was set at its maximum available value at all times. However, during landing the thrust is less than the maximum value and can be used as a control variable. We use rotor shaft tilt and rotor thrust as two control variables. The simplified and linearized equations are

*Otherwise the pitch angle is determined by the requirement of zero normal acceleration.

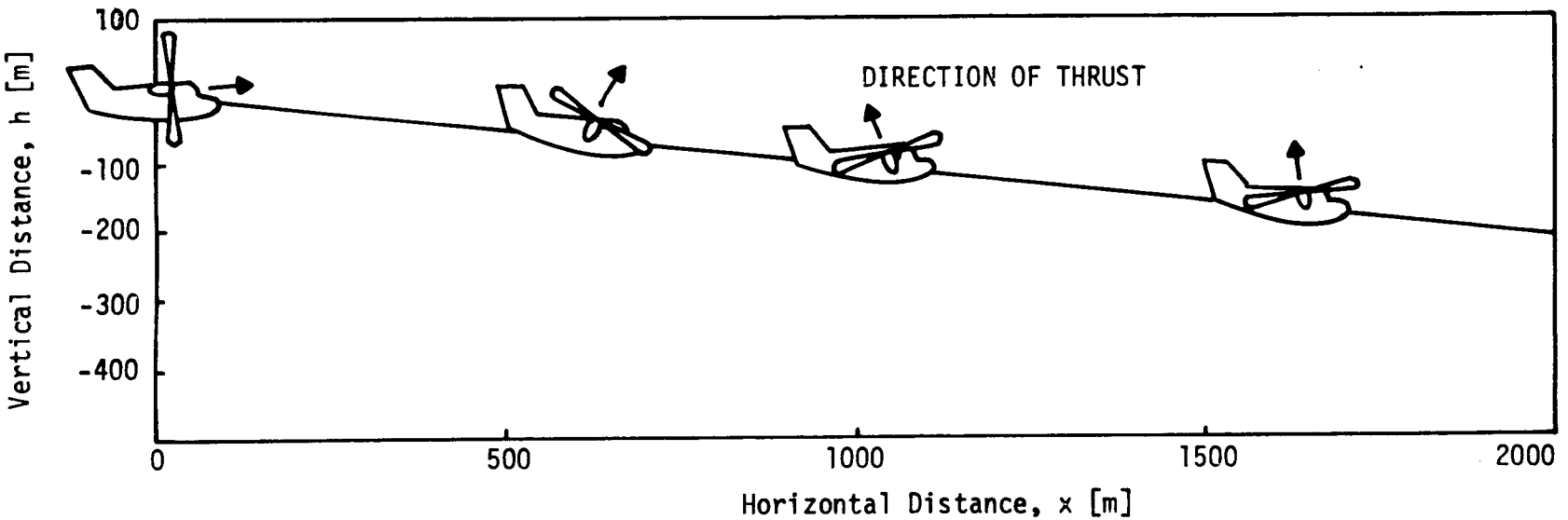

Figure 5.1 Nominal Landing Trajectory

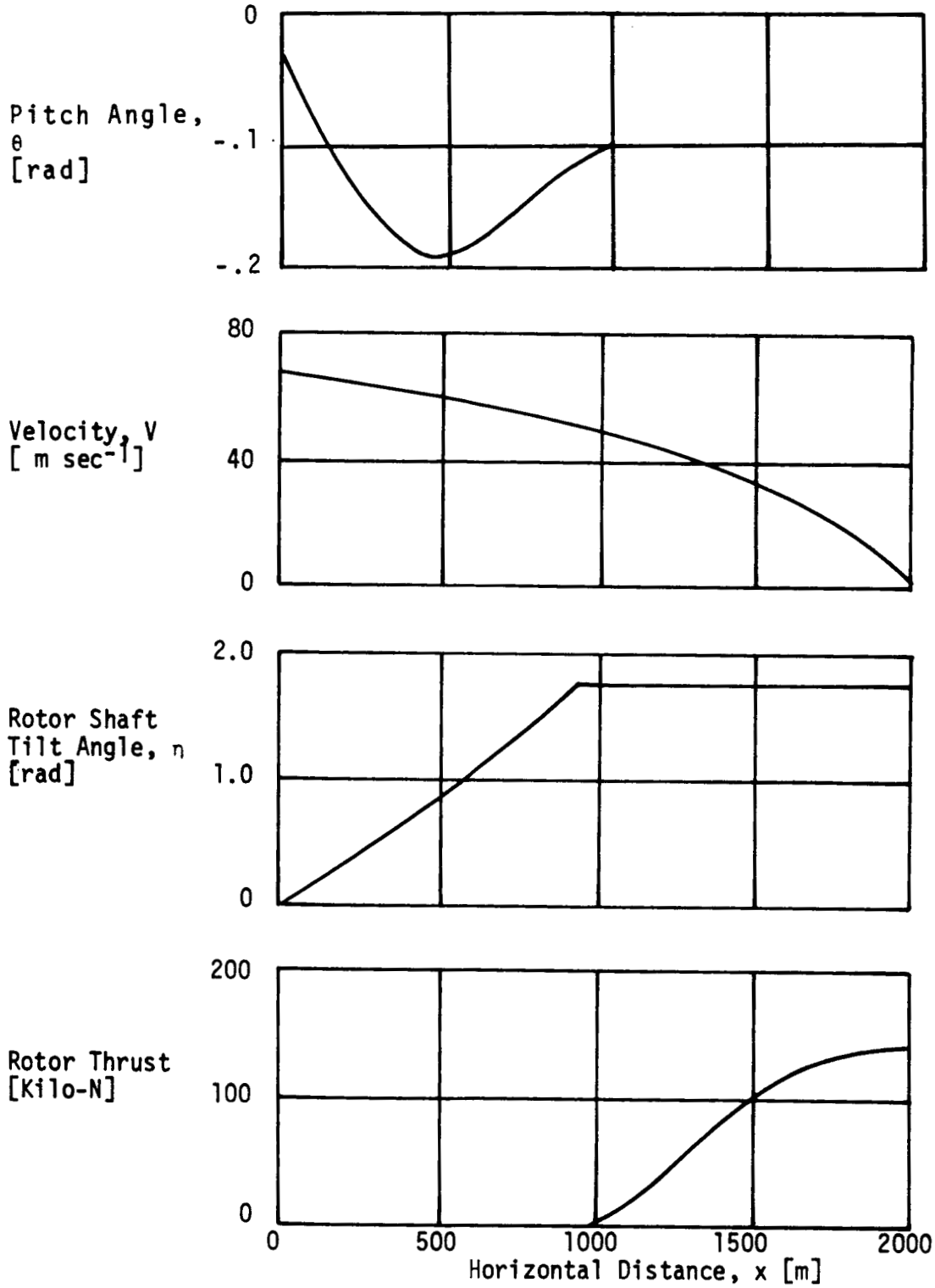

Figure 5.2 Velocity, Rotor Shaft Tilt and Rotor Thrust for the Nominal Trajectory

$$\frac{dZ_w}{dx} = F_w(x)Z_w + G_L(x)u_L \qquad (5.2.1)$$

where

$$G_L = \begin{Bmatrix} g_{1\eta} & g_{1T} \\ g_{2\eta} & g_{2T} \\ 0 & 0 \\ 0 & 0 \end{Bmatrix}$$

and

$$u_L = \begin{bmatrix} \delta\eta \\ \delta T \end{bmatrix} \qquad (5.2.2)$$

5.3 Choice of Weighting Matrices

The technique for choosing weighting matrices is very similar to the take-off case and is described in Section 4.3. The final values of A, B and S_{x_f} are (units meters, sec, rad)

$$A = \begin{bmatrix} .0011 & 0 & 0 & 0 \\ 0 & .04 & 0 & 0 \\ 0 & 0 & .00044\cos^2\gamma & 0 \\ 0 & 0 & 0 & 0 \end{bmatrix}$$

$$B^{-1} = \begin{bmatrix} .082V & 0 \\ 0 & 2\times10^7 V \end{bmatrix}$$

and,

$$S_{x_f} = \left\{ \begin{array}{cccc} .36 & .065 & -.0036 & -.04 \\ .065 & .032 & .0044 & -.06 \\ -.0036 & .0044 & .0072 & -.057 \\ -.04 & -.06 & -.057 & 240 \end{array} \right\}^{*} \qquad (5.3.1)$$

5.4 Gains and Flight Paths in the Presence of Wind

Figures 5.3 and 5.4 show gains on rotor shaft tilt and thrust as a function of the horizontal distance. Near the terminal point, the optimal gains had wide fluctuations in spite of choosing S_{x_f} given above. The gains have been smoothed in this region.

Notice that gains on rotor shaft tilt are zero for $x < 930$ m. For this range of x the nominal thrust is zero. Hence changing the rotor shaft tilt produced no change in forces.

Unlike the take-off guidance some gains in this case are positive. There are two main reasons for this: (a) Since the landing trajectory is a straight line the velocity-dependent centrifugal force is absent, (b) during a major portion of the flight the rotor shaft is tilted more than 90°; under this condition increasing the rotor shaft tilt produces many effects which are similar to the effects produced by decreasing the rotor shaft tilt if it were less than 90°.

In the absence of the centrifugal force, it is much easier to explain the nature of the control gains. If the rotor shaft tilt exceeds 90°, increasing it decreases the force along the velocity vector and perpendicular to the

*In this case S_{x_f} is computed using w=-.0001w+"white" noise to avoid the problem of zero eigenvalue in the eigenvector decomposition technique.

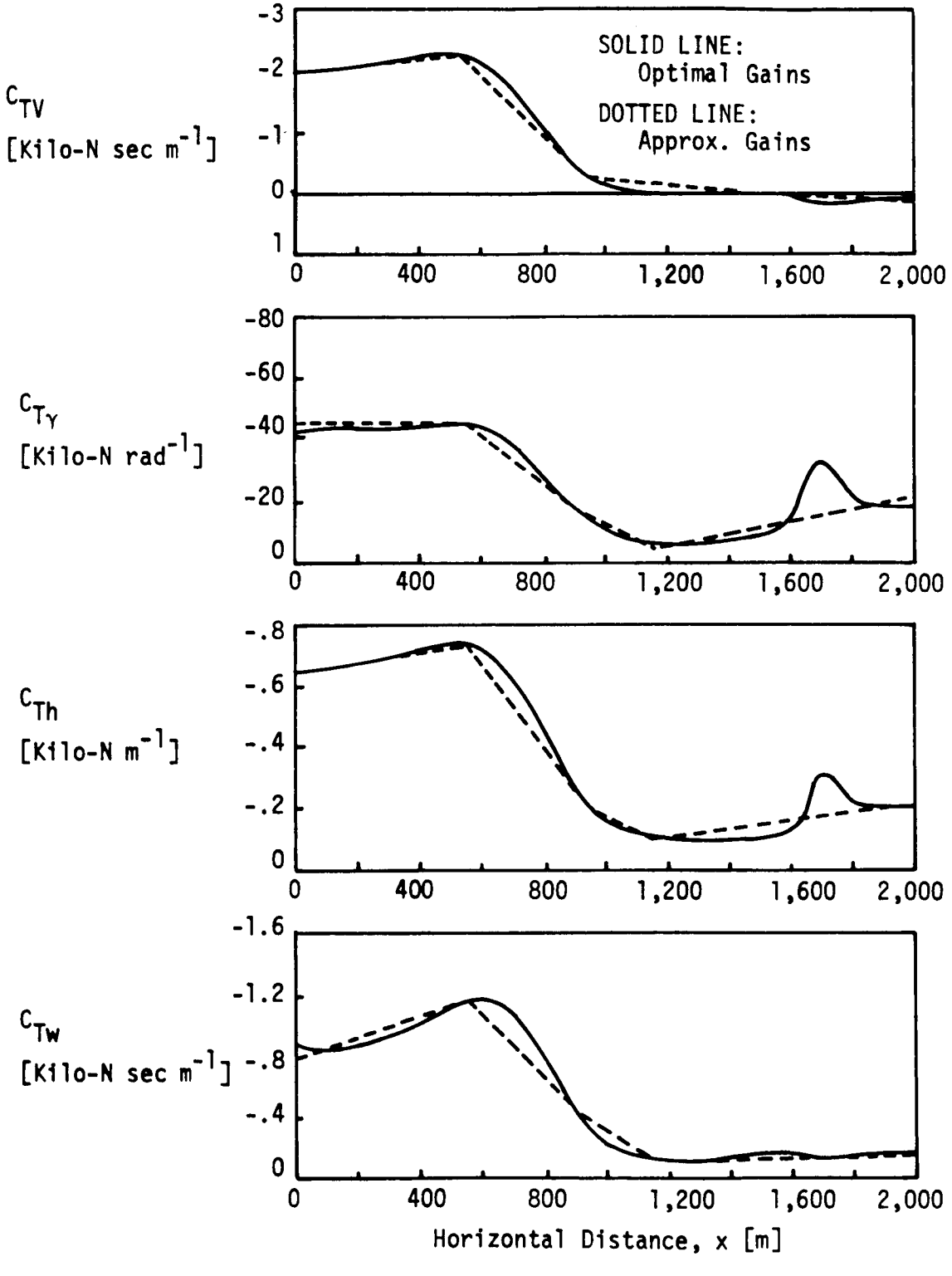

Figure 5.3 Gains on Rotor Thrust

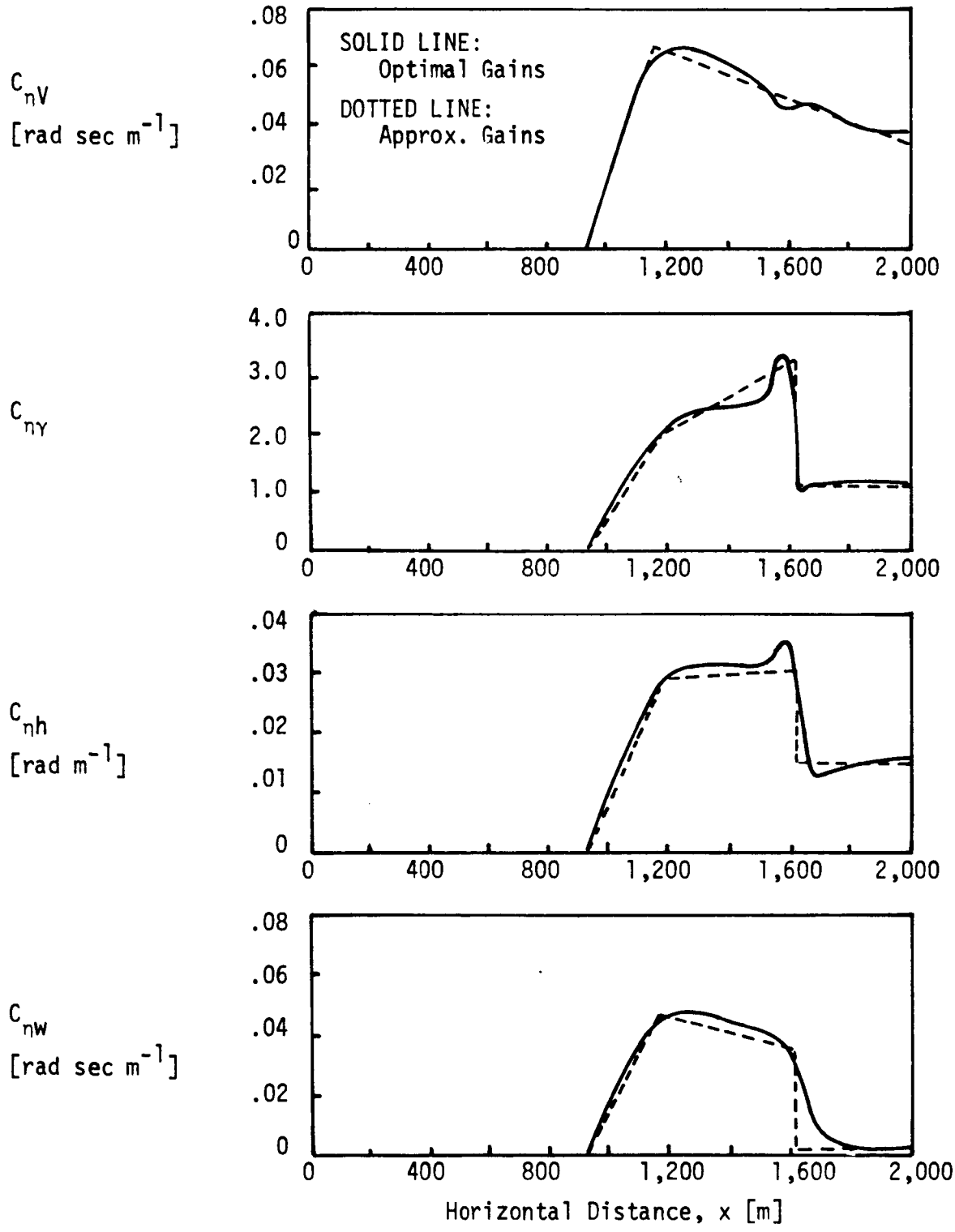

Figure 5.4 Gains on Rotor Shaft Tilt Angle

velocity vector. This tends to reduce velocity, flight path angle and height. Hence $C_{\eta V}$, $C_{\eta \gamma}$ and $C_{\eta h}$ are positive or zero.

The gains on rotor thrust are never zero. It is assumed that it is possible to produce small negative thrusts. During the initial part of the trajectory when the rotor tilt is less than 90°, an increase in thrust increases the force along the velocity and perpendicular to the velocity. Thus C_{TV}, $C_{T\gamma}$ and C_{Th} are negative. As the rotor tilt exceeds 90°, C_{TV} tends to change sign.

A positive wind velocity (head-wind) has two effects. It decreases the angle of attack (because the nominal flight path angle is negative) and increases the air speed. It is not straight forward to predict the signs of $C_{\eta w}$ and C_{Tw}.

Figure 5.5 shows the errors in velocity and the distance perpendicular to the nominal flight path for an initial error of -0.1 radian in flight path angle and -5 m in vertical distance. This is a large error since it increases the angle of attack by 5.7°. The error in velocity increases to about 2 m sec^{-1} and then decreases. The distance normal to the nominal flight path increases from -4.9 m to -12 m The aircraft reaches the terminal point with a small error in position and a small velocity in the forward direction. The figure also shows $\delta\eta$ and δT. The change in thrust starts from a high positive value and soon decreases to a low value. The $\delta\eta$ never exceeds 2.5°. With no control the velocity would be 5.1 m sec^{-1} and distance normal to nominal trajectory would be -9.5 m at the terminal point.

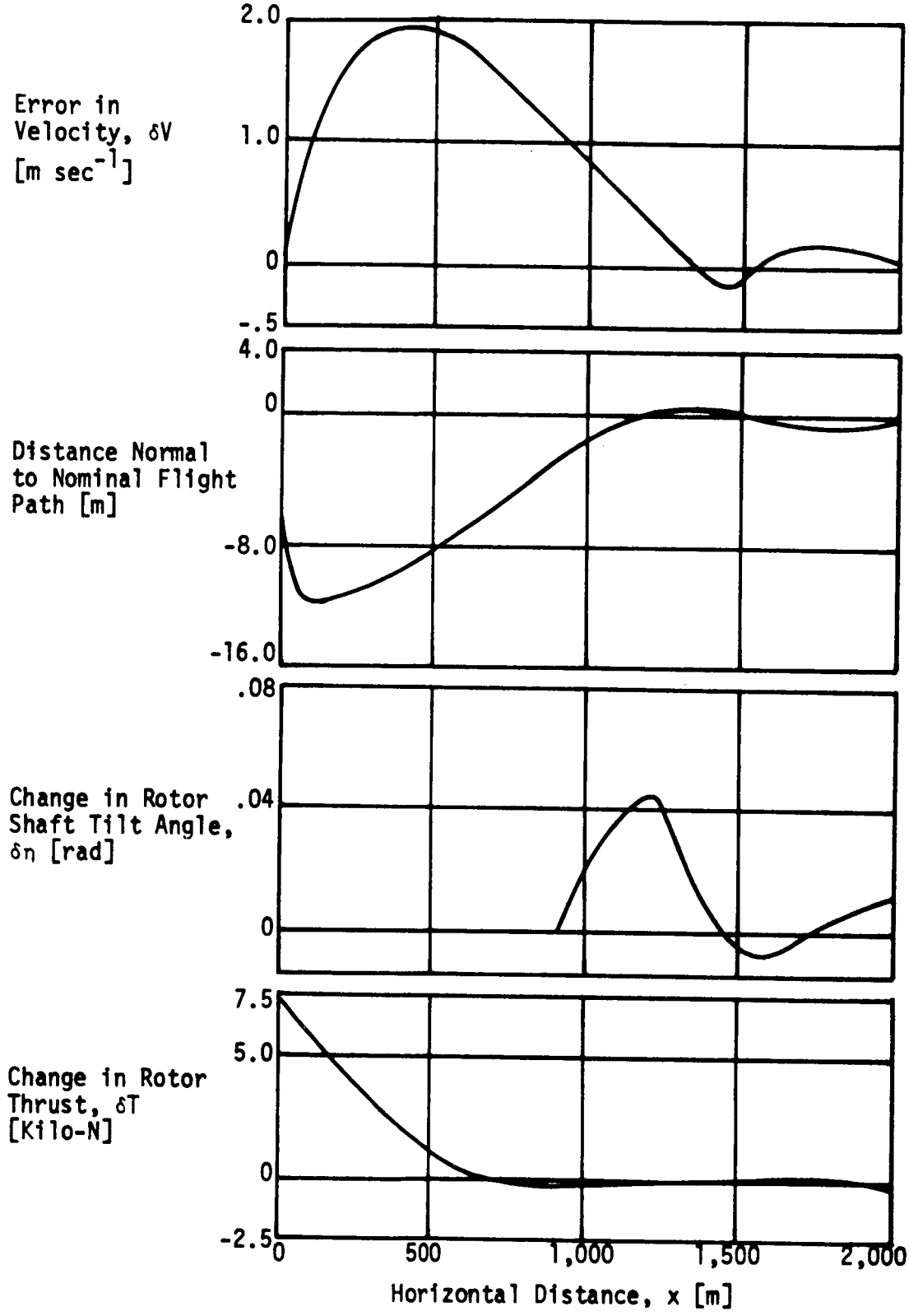

Figure 5.5 Errors and Control Effort with Initial Errors in Position and Flight Path Angle

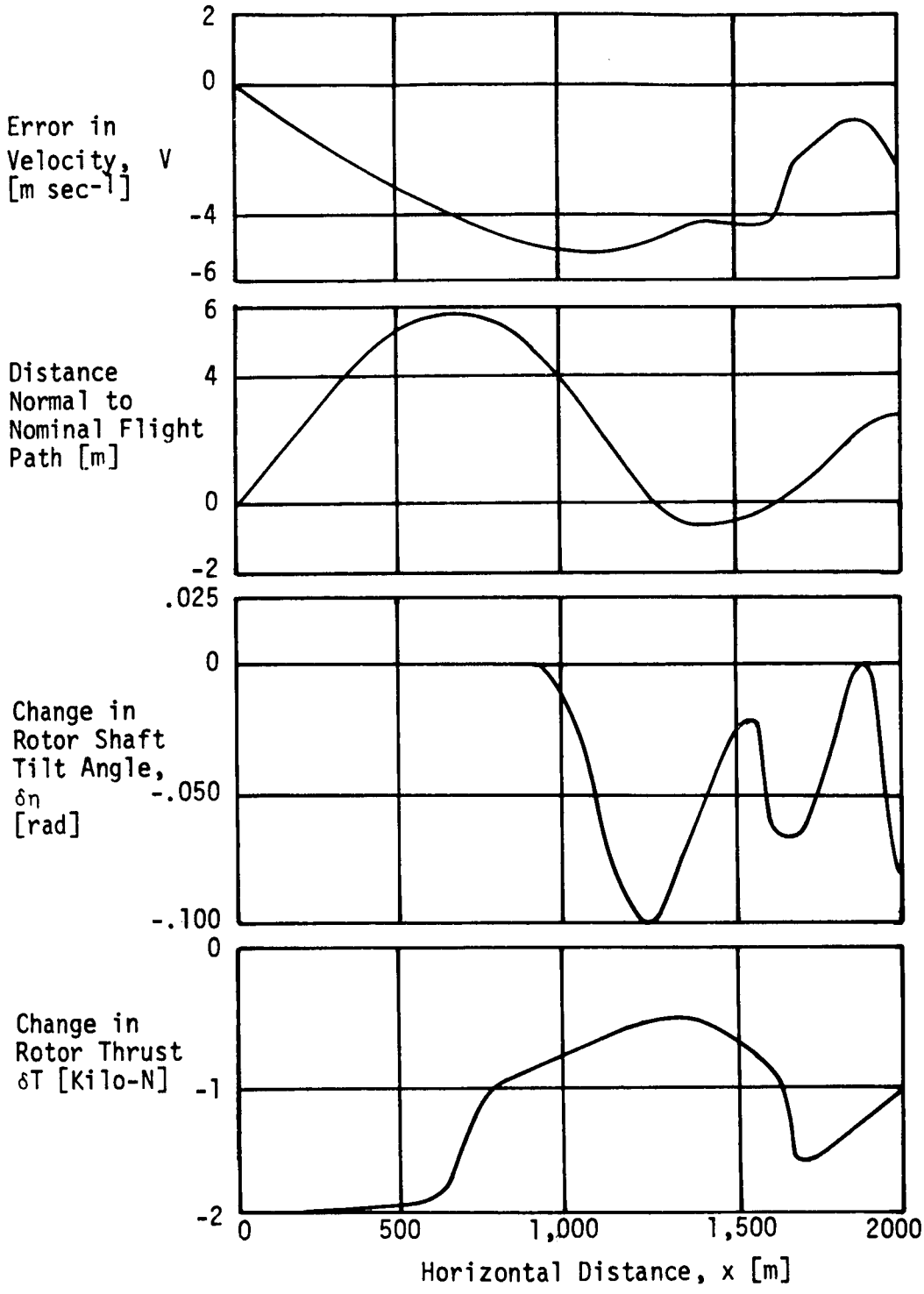

Figure 5.6 Errors and Control Effort in the Presence of Head Wind

Figure 5.6 is a similar diagram when the aircraft flies in a constant head-wind of 5.0 m sec^{-1} with no initial errors. In the absence of feedback control the aircraft never reaches the terminal point. The forward velocity is zero 165 m away from this point and the position error (distance normal to the nominal trajectory) is -80 m. With feedback control the error in velocity never exceeds 6 m sec^{-1} and distance normal to the nominal trajectory is always less than 6.0 m. The aircraft comes to rest 3 m away from the terminal point and the error in position is 2.8 m. In this computation all state variables are assumed to be known exactly except the wind velocity. The wind velocity is estimated using the technique of Section 3.5 with a filter of time constant 4 sec. The maximum value of $|\delta\eta|$ is 5.7° and the maximum value of $|\delta T|$ is about 2000 N. As in the case of take-off the controlled trajectories were computed using the nonlinear equations.

Figures 5.7 and 5.8 show RMS values of state and control variables as a function of the horizontal distance, x, in the presence of a horizontal wind with two components: (a) a steady wind with 3.0 m sec^{-1} RMS value plus (b) a random wind with 3.0 m sec^{-1} RMS value and .30 sec correlation time. RMS values of initial errors in velocity, flight path angle and vertical distance are taken as 1.0 m sec^{-1}, .01 rad and 3.0 m respectively. The linearized equations are used for this computation since the use of nonlinear equations makes it necessary to use the expensive Monte-Carlo type simulation.

The RMS errors in velocity and position increase initially, decrease and then increase again near the terminal point. These errors are always reasonably small. The error in flight path angle stays small rising to a very high value when the aircraft speed is small. The control effort required to obtain this performance is quite reasonable.

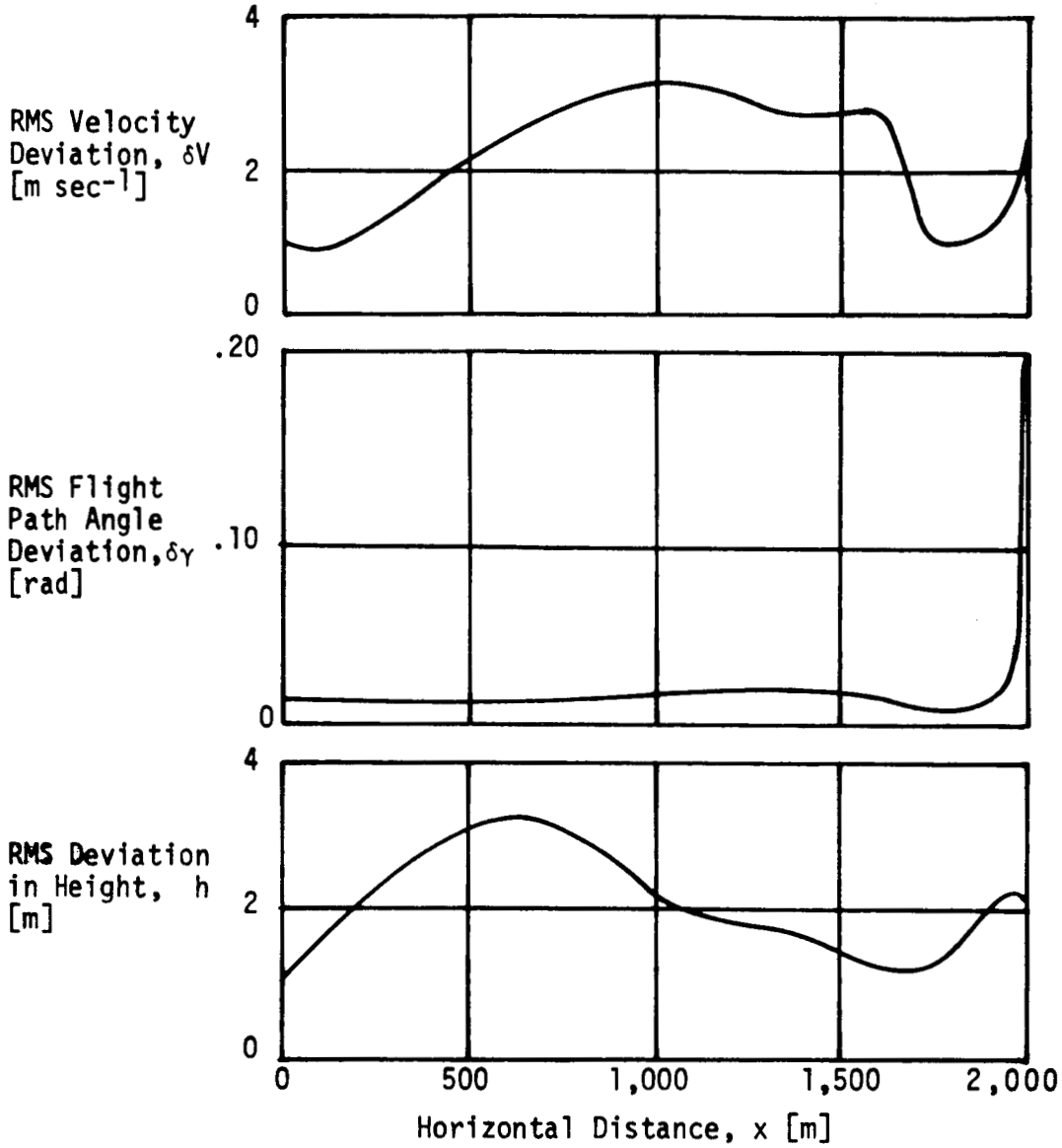

Figure 5.7 RMS State in the Presence of Random Wind, w
[$w=w_1+w_2$, w_1=random bias (RMS 3 $msec^{-1}$),
w_2=white noise, power spectral density=5.4 m^2sec^{-1}]

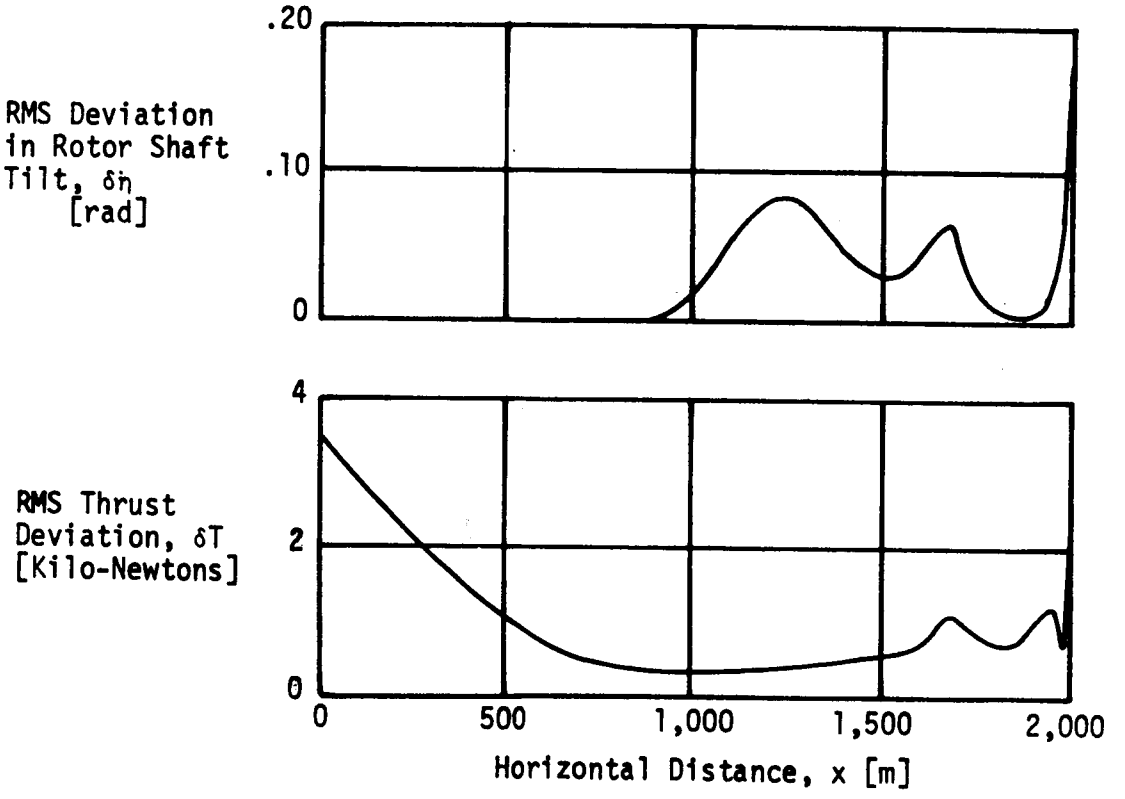

Figure 5.8 RMS Control in the Presence of Random Wind of Figure 5.7

5.5 Summary

Most of the control gains obtained in this chapter can be approximated by a combination of constant values and ramp functions. It is necessary to do this to save computation time and required memory on an airborne computer. The approximated gains are shown in dotted lines in Figures 5.3 and 5.4.

The performance of the optimal and the approximated gains in the presence of initial disturbances in velocity and flight path angle is compared in Table V-1. The tilting proprotor VTOL aircraft has about the same terminal and average error with optimal and with approximate gains. There is a considerable improvement especially in terminal velocity and position through using the feedback control.

Table V-2 shows the VTOL behavior in the presence of 5.0 m sec^{-1} head wind. There is a significant improvement in performance when there is a feedback on wind velocity. The use of approximate gains deteriorates the performance slightly. With no feedback control the errors are so large that it seems impossible to land the aircraft.

CONTROL SYSTEM	DEVIATION NORMAL TO THE NOMINAL TRAJECTORY		VELOCITY AT TERMINAL POINT	DEVIATION IN ROTOR SHAFT TILT ANGLE		DEVIATION IN THRUST	
	Ave Value*	Terminal Value		Max Value	Ave Value*	Max Value	Ave Value*
Optimal Gains	3.6 m	.16 m	.04 $m.sec^{-1}$	2.5°	.41°	7500 N	800 N
Approx Gains	3.6 m	.18 m	.045 $m\ sec^{-1}$	2.40°	.40°	7900 N	790 N
No Control	11 m	9.5 m	5.1 $m\ sec^{-1}$	-	-	-	-

* Average over horizontal distance x

Table V-1 System Performance in the Presence of Initial Disturbances

	Gains Approx	Exact Wind Vel	Wind Vel Observer	DEVIATION NORMAL TO THE NOMINAL FLIGHT PATH		DISTANCE FROM TERMINAL POINT WHERE VELOCITY IS ZERO	DEVIATION IN ROTOR SHAFT TILT ANGLE		DEVIATION IN THRUST	
				Ave Value*	Terminal Value		Max Value	Ave Value*	Max Value	Ave Value*
1	No	No	No	6.6 m	4.9 m	5.2 m	5.2°	1.4°	2300 N	640 N
2	No	Yes	No	2.3 m	2.7 m	2.8 m	6.6°	1.6°	4400 N	1100 N
3	No	No	Yes	2.8 m	2.7 m	3.0 m	5.7°	1.4°	2000 N	1200 N
4	Yes	No	No	6.7 m	4.8 m	6.4 m	6.3°	1.5°	1500 N	560 N
5	Yes	Yes	No	2.4 m	3.0 m	4.0 m	6.6°	1.5°	3900 N	1100 N
6	Yes	No	Yes	2.9 m	3.0 m	4.2 m	5.7°	1.3°	2100 N	1100 N
	NO CONTROL			9.2 m	80 m	165 m	-	-	-	-

*Average over horizontal distance x

Table V-2 Comparison of Different Controls in the Presence of 5.0 m sec^{-1} Head-Wind

CHAPTER VI
Lateral Guidance

6.1 Equations of Motion

The lateral motions (sideslip, β, roll angle, ϕ, and yaw angle, ψ) of a tilt-rotor aircraft are nearly uncoupled from the longitudinal motions just as in the case of conventional aircraft. In general these three motions are coupled. In the absence of wind, these equations for small β, ϕ and ψ, are the same as for a conventional aircraft (BL-1),

$$\begin{Bmatrix} \frac{mV}{Sq_d}s - C_{y_\beta} & \left(\frac{mV}{Sq_d} - C_{y_r}\right)s - C_{y_\psi} & -C_{y_\phi} \\ -C_{n_\beta} & \frac{I_z}{Sq_d b}s^2 - \frac{b}{2V}C_{n_r}s & -\frac{J_{xz}}{Sq_d b}s^2 - \frac{b}{2V}C_{n_p}s \\ -C_{\ell_\beta} & -\frac{J_{xz}}{Sq_d b}s^2 - \frac{b}{2V}C_{\ell_r}s & \frac{I_x}{Sq_d b}s^2 - \frac{b}{2V}C_{\ell_p}s \end{Bmatrix} \begin{Bmatrix} \beta \\ \psi \\ \phi \end{Bmatrix}$$

$$= \begin{Bmatrix} C_y \\ C_n \\ C_\ell \end{Bmatrix} \qquad (6.1.1)$$

Defining,

$$\varepsilon \triangleq \beta + \psi \qquad (6.1.2)$$

equations (6.1.1) can be written in another form in the presence of a lateral wind w_y (see Figure 6.1).

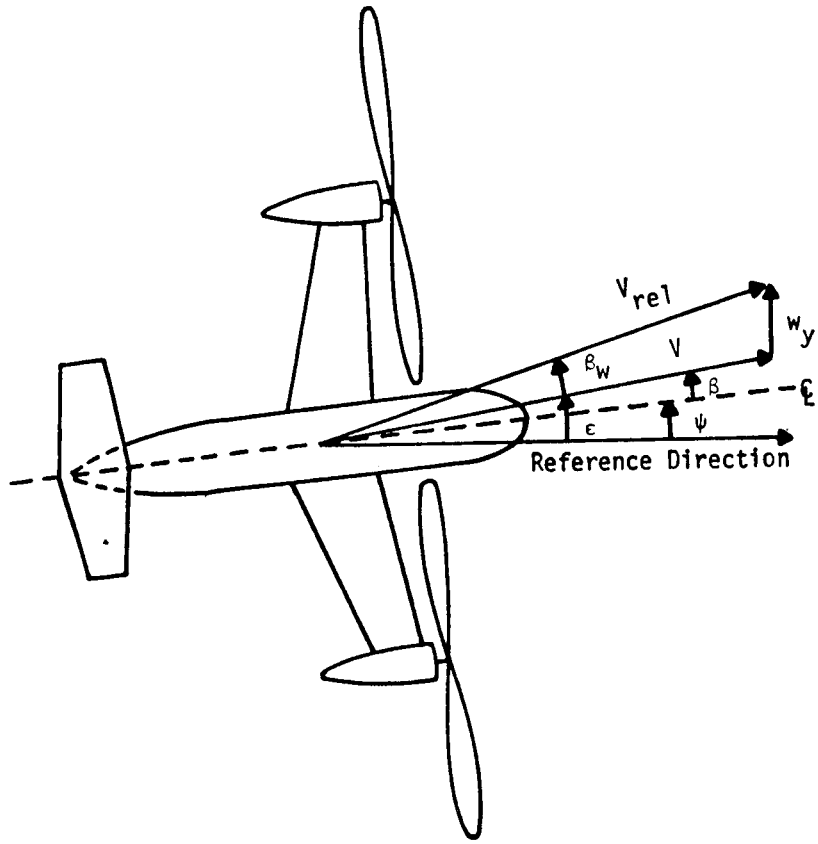

Figure 6.1 Lateral Motions of Tilt Rotor Aircraft

$$\dot{\varepsilon} = -C_1(\varepsilon-\psi+\frac{w_y}{V})+C_2\phi+C_1'\psi+b_1Y$$

$$\ddot{\psi} = -\omega_0^2(\psi-\varepsilon-\frac{w_y}{V})-C_3\dot{\psi}+C_4\dot{\phi}+b_2N$$

$$\ddot{\phi} = -C_5\dot{\phi}-C_6(\psi-\varepsilon-\frac{w_y}{V})+C_7\dot{\psi}+b_3L \qquad (6.1.3)$$

where C_{y_r}, J_{xz}/Sq_db are small and have been neglected and

$$C_1 = -\frac{C_{y_\beta}}{mV/Sq_d} \quad , \quad C_1' = +\frac{C_{y_\psi}}{mV/Sq_d} \quad , \quad C_2 = \frac{C_{y_\phi}}{mV/Sq_d}$$

$$b_1 = \frac{1}{mV} \quad , \quad \omega_0^2 = -\frac{C_{n_\beta}}{I_z/Sq_db} \quad , \quad C_3 = -\frac{\frac{b}{2V}C_{n_r}}{I_z/Sq_db}$$

$$C_4 = \frac{\frac{b}{2V} C_{n_p}}{I_z/Sq_d b} \quad , \quad b_2 = \frac{1}{I_z} \quad , \quad C_5 = -\frac{\frac{b}{2V} C_{\ell_p}}{I_x/Sq_d b}$$

$$C_6 = \frac{C_{\ell_r}}{I_x/Sq_d b} \quad ; \quad C_7 = \frac{\frac{b}{2V} C_{\ell_r}}{I_x/Sq_d b} \quad , \quad b_3 = \frac{1}{I_x}$$

(6.1.4)

Y is the control side force (if there is one) and N and L are control moments about the yaw and roll axes respectively. In a tilt-rotor aircraft direct side force could be produced by a simultaneous lateral cyclic pitch change in both rotors. However to avoid this additional complication in design, we shall instead use differential collective pitch to give a control rolling moment.

The lateral distance away from the nominal flight path, y, is given by

$$\dot{y} = V \varepsilon \tag{6.1.5}$$

Yaw moment is produced by differential rotor shaft tilt or differential cyclic pitch variation in the longitudinal direction. Large moments can be generated quickly because of high available thrust. Thus the roll and yaw angles can be changed much faster than the lateral deviation, y. In other words ε,y motions occur at lower frequencies (or larger time constants) than the ϕ,ψ motions. Therefore, we can approximately decouple the lateral equations into two systems.

$$\begin{aligned} \ddot{\psi} + C_3\dot{\psi} + \omega_0^2\psi + C_4\dot{\phi} &= b_2 N + \omega_0^2(\varepsilon + \frac{w_y}{V}) \\ \ddot{\phi} + C_5\dot{\phi} - C_7\dot{\psi} + C_6\psi &= b_3 L + C_6(\varepsilon + \frac{w_y}{V}) \end{aligned} \tag{6.1.6}$$

and,

$$\dot{\varepsilon}+C_1\varepsilon = (C_1+C_1')\psi+C_2\phi+C_1\frac{w_y}{V} \qquad (6.1.7)$$

$$\dot{y} = V\varepsilon$$

In (6.1.7) we may treat ψ and ϕ as control variables.

The lateral wind velocity can be approximated by a first order system excited by a white noise, i.e.,

$$\tau\dot{w}_y+w_y = \eta \qquad \overline{\eta(t)} = 0 \qquad \text{and} \quad \overline{\eta(t)\eta(\tau)} = Q\delta(t-\tau) \qquad (6.1.8)$$

6.2 Outer Loop Control Gains

The outer loop of the lateral guidance scheme is defined by equations (6.1.7) and (6.1.8) in which a linear combination of ψ and ϕ, $\phi+(C_1+C_1')/C_2\ \psi$, is the control variable. For automatic take-offs and landings, it is necessary to control the lateral position. Writing these equations in terms of the lateral position away from the nominal flight path.

$$\ddot{y}+C_1\dot{y} = V(C_1+C_1')\psi+VC_2\phi+C_1w_y \qquad (6.2.1)$$

$$\tau\dot{w}_y+w_y = \eta$$

Let us choose

$$\phi+\frac{(C_1+C_1')}{C_2}\psi = -k_1y-k_2\dot{y}-k_3w_y \qquad (6.2.2)$$

Then we have

$$\ddot{y}+C_1\dot{y} = VC_2(-k_1y-k_2\dot{y}-k_3w_y)+C_1w_y \qquad (6.2.3)$$

$$\tau\dot{w}_y+w_y = \eta$$

The first of equations (6.2.3) is a second order system forced by w_y. A good choice for control gain k_3 is obtained

by putting the coefficient of w_y in this equation equal to zero, i.e.,

$$k_3 = \frac{C_1}{VC_2} = -\frac{Cy_\beta}{VC_{y_\phi}} \qquad (6.2.4)$$

There are several methods for choosing the other gains. One method is to choose the gains in such a way that it becomes a constant coefficient second order system. If ω_y and ξ_y are the desired natural frequency and damping ratio respectively,

$$k_1 = \frac{\omega_y^2}{VC_2} = \frac{\omega_y^2}{VC_{y_\phi}} \frac{mV}{Sq_d}$$

$$k_2 = \frac{1}{VC_2}(2\xi_y\omega_y - C_1) = \frac{2\xi_y\omega_y}{VC_2} + \frac{C_{y_\beta}}{C_{y_\phi}} \frac{1}{V} \qquad (6.2.5)$$

Expressions for C_{y_β}, C_{y_ϕ} and C_{y_ψ}

C_{y_β} is the coefficient governing the rate of change of side force with sideslip. It is given by (BL-1)

$$C_{y_\beta} = \frac{1}{Sq_d} \frac{\partial F_y}{\partial \beta} \qquad (6.2.6)$$

C_{y_β} is almost constant and is usually negative. Its value for the tilt rotor aircraft under consideration is not available. A value of -.6 was estimated.

If θ is the pitch angle the stability derivatives C_{y_ϕ} and C_{y_ψ} are,

$$C_{y_\phi} = \frac{mg}{Sq_d} \cos\theta$$

$$C_{y_\psi} = \frac{mg}{Sq_d} \sin\theta \qquad (6.2.7)$$

Let us pick control gains to obtain a natural frequency of 0.25 rad sec^{-1}.and a damping ratio of 0.707

$$k_1 = \frac{(.25)^2}{Vg \cos\theta} \qquad V = \frac{(.25)^2}{9.81 \cos\theta} = \frac{.0064}{\cos\theta} \text{ rad } m^{-1}$$

$$k_2 = \frac{.3535}{g \cos\theta} + \frac{(-.6)\times Sq_d}{mg \cos\theta}\frac{1}{V}$$

$$= \left\{\frac{.036}{\cos\theta} - \frac{1.1\times10^{-4}V}{\cos\theta}\right\} \text{ rad sec } m^{-1}$$

$$k_3 = \frac{1.1\times10^{-4}V}{\cos\theta} \text{ rad sec } m^{-1} \qquad (6.2.8)$$

During a major portion of the take-off trajectory the pitch angle is 20° and for the landing trajectory is -5.7°. These angles are used in expressions (6.2.8). The controller gains for take-off and landing are shown in Table VI-1.

The small angle approximation for sideslip is not good at low speeds. This problem is reduced by writing the equations in the form (6.2.1) and (6.1.6) and redefining some stability derivatives. Though the sideslip angle may be large at low speeds, the lateral displacement and lateral velocity are usually small. However, the decoupling assumption is at best approximate when the speed is very low.

6.3 Inner Loop Control Gains

Equations (6.1.6) and (6.1.8) define the equations governing the inner loop dynamics for the lateral motion.

GAIN	TAKE-OFF	LANDING
K_1 rad m^{-1}	.0066	.0065
K_2 rad m^{-1}sec	$.037 - 1.1 \times 10^{-4}V$	$.036 - 1.1 \times 10^{-4}V$
K_3 rad m^{-1}sec	$1.1 \times 10^{-4}V$	$1.1 \times 10^{-4}V$

Table VI-1 Outer Loop Control Gains for Take-off and Landing

These differential equations for ϕ and ψ are coupled and are forced by ε and w_y. The coefficient C_4 is usually small and the coupling is approximately one way.

The required value of $\phi+((C_1+C_1')/C_2)\psi$ at any time is given by equation (6.2.2). The choice of either ϕ or ψ is arbitrary as long as this equation is satisfied. The control system will be designed to maintain a zero yaw angle.

Making the assumption of one way coupling for choosing control gains, let

$$N = -k_4\psi - k_5\dot{\psi} - k_6(\varepsilon V + w_y) + \frac{C_4}{b_2}\dot{\phi} \qquad (6.3.1)$$

then

$$\ddot{\psi} + (C_3 + b_2 k_5)\dot{\psi} + k_4 b_2 \psi = \left(\frac{\omega_0^2}{V} - k_6 b_2\right)(\varepsilon V + w_y) \qquad (6.3.2)$$

If we require a natural frequency ω_ψ and damping ratio ξ_ψ, a good choice for the gains is,

$$k_4 = \frac{\omega_\psi^2}{b_2} = \omega_\psi^2 I_z$$

$$k_5 = (2\xi_\psi\omega_\psi - C_3)\frac{1}{b_2} = 2\xi_\psi\omega_\psi I_z + \frac{b}{2V}C_{n_r}\, Sq_d b \qquad (6.3.3)$$

$$k_6 = \frac{\omega_0^2}{(Vb_2)} = \frac{C_{n_\beta}\, Sq_d b}{V}$$

Let $\omega_\psi = 1.5$ rad sec^{-1} and $\xi_\psi = 0.707$

$$k_4 = 2.25\, I_z = 2.4 \times 10^5 \text{ N m rad}^{-1}$$

$$k_5 = 2.121\ I_z + 2530\ C_{n_r} V$$

$$= (2.2 \times 10^5 + 2.5 \times 10^3 C_{n_r} V) \text{N m sec rad}^{-1}$$

$$k_6 = 337\ C_{n_\beta} V \text{ N sec rad}^{-1}$$

The second of equations (6.1.6) is of second order in ϕ and is excited by a linear combination of ψ, $\dot{\psi}$ and $(w_y + \varepsilon V)$. We can choose

$$L = -k_7\phi - k_8\dot{\phi} - k_9(\varepsilon V + w_y) - \frac{C_7}{b_3}\dot{\psi} + \frac{C_6}{b_3}\psi \qquad (6.3.5)$$

The equation for roll angle becomes

$$\ddot{\phi} + (C_5 + b_3 k_8)\dot{\phi} + b_3 k_7 \phi = \left(\frac{C_6}{V} - b_3 k_9\right)(\varepsilon V + w_y) \qquad (6.3.6)$$

As before, if ω_ϕ and ξ_ϕ are the required natural frequency and damping ratio respectively, the gains become

$$k_7 = \frac{\omega_\phi^2}{b_3} = I_x \omega_\phi^2$$

$$k_8 = \frac{1}{b_3}(2\xi_\phi \omega_\phi - C_5) = 2\xi_\phi \omega_\phi I_x + \frac{b}{2V} C_{\ell_p} Sq_d b$$

$$k_9 = \frac{C_6}{V b_3} = \frac{C_{\ell_\beta} Sq_d b}{V}$$

with

$$\omega_\phi = 1.5 \text{ rad sec}^{-1} \quad \text{and} \quad \xi_\phi = 0.707$$

the control gains become,

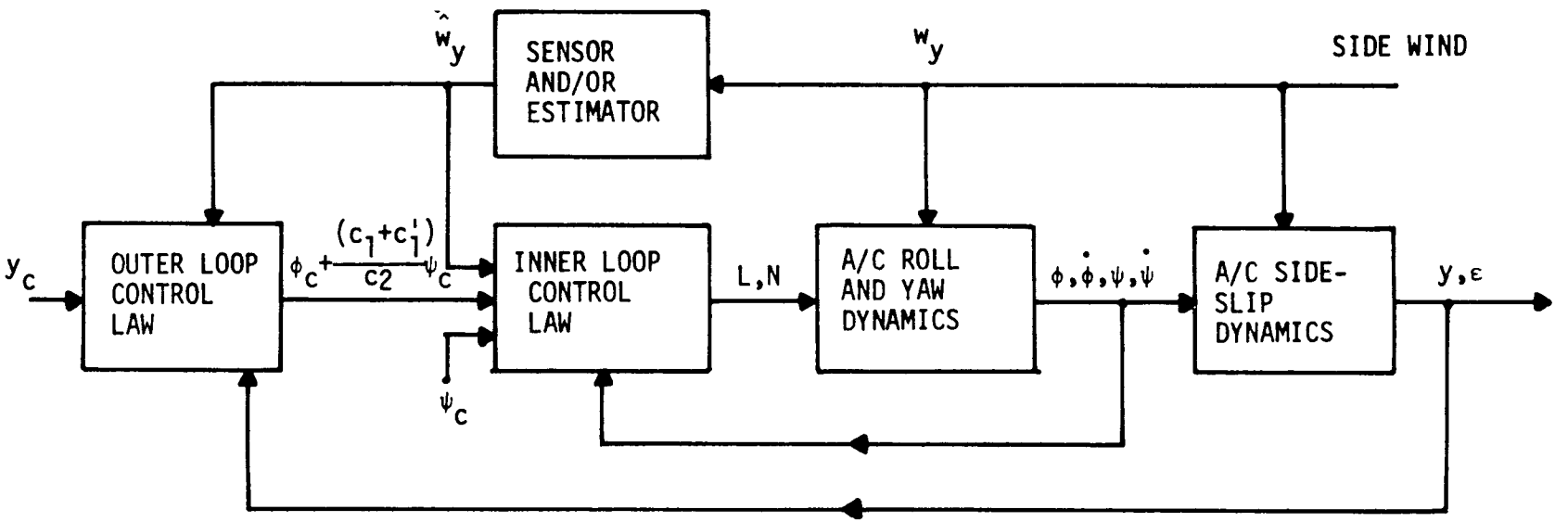

$( )_c = ( )_{command}$

Figure 6.2 The Complete Lateral Control System

$$k_7 = 2.25\ I_x = .7\times10^5\ \text{N m rad}^{-1}$$

$$k_8 = 2.121\ I_x + 2530\ C_{\ell_p} V$$

$$= (.67\times10^5 + 2530\ C_{\ell_p} V)\ \text{N m sec rad}^{-1} \quad (6.3.8)$$

$$k_9 = 337\ C_{\ell_\beta} N\ \text{sec rad}^{-1}$$

Stability derivatives C_{n_r}, C_{n_β}, C_{ℓ_p} and C_{ℓ_β} are functions of flight parameters. These data are not available for Bell Model 266 tilting proprotor aircraft. Therefore the gains have not been computed. However, the above equations show the order of magnitude of these gains. Once these stability derivatives are available the gains can be computed as a function of the independent variable, x.

A block diagram of the control system for lateral control is shown in Figure 6.2.

REFERENCES

BE-1 Model 266 Composite Aircraft Program Technical Volume, Bell Helicopter Report 266-099-202 prepared for U.S. Army Aviation Materiel Lab., Fort Eustis under Contract DAAJ02-67-C-0044.

BL-1 John H. Blakelock, Automatic Control of Aircraft and Missiles, John Wiley and Sons, Inc., New York, 1965.

BR-1 Arthur E. Bryson, Jr. and Yu-Chi Ho, Applied Optimal Control, Blaisdell Publishing Company, Waltham, Massachusetts, 1969.

BR-2 Arthur E. Bryson, Jr. and W. Earl Hall, Jr., Synthesis of Hover Autopilots for Rotary-Wing VTOL Aircraft, Stanford University Department of Aeronautics and Astronautics, Report No. 446, June 1972.

BU-1 R. Bulirsch, and J. Stoer, Numerical Treatment of Ordinary Differential Equations by Extrapolation Methods, Numerische Mathematik 8, 1-13 (1966).

GE-1 A. Gessow, and G.C. Myers, Jr., Aerodynamics of the Helicopter, The McMillan Company, New York, 1952.

HA-1 R. Hafner, The Case for the Convertible Rotor, The Aeronautical Journal of the Royal Aeronautical Society, Vol. 75, August 1971, pp. 505-528.

HO-1 S.F. Hoerner, Fluid Dynamic Drag: Practical Information on Aerodynamic Drag and Hydrodynamic Resistance, Bricktown, N.J., 1965.

NI-1 Nikolsky, X. Helicopter Analysis, New York, John Wiley and Sons, 1951.

PE-1 C.D. Perkins and R.E. Hage, Airplane Performance Stability and Control, New York, John Wiley and Sons, January 1967.

SH-1 F.H. Schmitz, W.Z. Stepniewski, J. Gibs, and E. Hintekenser, A Comparison of Optimal and Noise Abatement Trajectories of a Tilt-Rotor Aircraft, NASA CR-2034, May 1972.

APPENDIX A

Summary of Basic Data for Bell Model 266 Tilting-Proprotor VTOL Aircraft

General	
Overall length	17.0 m
Overall width (proprotors turning)	26.0 m
Distance between pylon pivot points	14.3 m
No. of engines	2
Shaft horse power (min)	3435 each (59° day)
	3370 each (92° day)
Helicopter Mode	
Hovering ceiling, out of ground effect (design TOW)	3870 m (standard day)
	2325 m (95° day)
Maximum speed (sea level, design TOW)	316 Km hr^{-1} (Twin engine)
	259 Km hr^{-1} (Single engine)
High Speed Mode	
Maximum speed (sea level, design TOW)	654 Km hr^{-1} (Twin engine)
	470 Km hr^{-1} (Single engine)
Maximum speed (3000 m, design TOW)	657 Km hr^{-1} (Twin engine)
	505 km hr^{-1} (Single engine)
Average cruise speed (design TOW)	408 Km hr^{-1} (Sea level)
	443 Km hr^{-1} (3,000 m)
	500 Km hr^{-1} (7,500 m)
Range (design TOW and payload)	820 Km

Wing

Area	35.5 m^2
Span	15.0 m
Aspect ratio	6.43
Airfoil section root	NACA 64-223, modified
tip	NACA 64-219, modified
Lift curve slope	4.28 rad^{-1}
Angle between wing zero lift line and fuselage axis	4.9°
Angle of attack at stall	17°
Aileron-flaps area/side	3.36 m^2
Flaps area/side	3.58 m^2
Wing loading	358 Kg m^{-2}

Proprotors

No. of proprotors	2
No of blades per proprotor	3
Radius	5.87 m
Disc area per proprotor	108.14 m^2
Blade area per proprotor	10.275 m^2
Blade chord	.585 m
Solidity	.095
Disc loading	58.6 Kg m^{-2}
Proprotor lock number	4.53

Fuselage

Length	16.1 m
Maximum breadth (less wheel fairings)	2.15 m
Area (Planform)	36.7 m^2

Horizontal Tail	
Area	9.4 m^2
Span	6.57 m
Aspect ratio	4.61
Lift curve slope	4.28 rad^{-1}
Airfoil section	NACA 64-012
Angle of incidence	-0.5°
Vertical Tail	
Area (including carry-through)	12.9 m^2
Span	5.5 m
Aspect ratio	2.34
Lift curve slope	2.75 rad^{-1}
Airfoil section root	NACA-64-015
tip	NACA-64-009
Weights	
Design take-off weight	12,700 Kg
Payload	2,990 Kg
Weight of rotors, pylons, engines etc. (Total)	3,175 Kg

APPENDIX B

Summary of the Longitudinal Equations of Motion and Weighting Matrices in the Quadratic Synthesis Technique

B.1 Nonlinear Equations

$$m \frac{dV}{dt} = - D_W - D_T - D_F - D_{NAC} - mg \sin \gamma + T \cos \phi - H \sin \phi$$

$$mV \frac{d\gamma}{dt} = + L_W + L_T + L_F + L_{NAC} - mg \cos \gamma + T \sin \phi + H \cos \phi$$

$$\frac{dx}{dt} = V \cos \gamma$$

$$\frac{dy}{dt} = V \sin \gamma$$

$$D_W = \frac{1}{2} \rho S_W V_R^2 [C_{D_W}(\alpha_R, \delta f) \cos (\Delta\alpha)$$

$$+ C_{L_W}(\alpha' - \Delta\alpha) \sin (\Delta\alpha)] \times .78 + \frac{1}{2} \rho S_W V^2 C_{D_W}(\alpha, \delta f) \times .22$$

$$L_W = \frac{1}{2} \rho S_W V_R^2 [- C_{D_W}(\alpha_R, \delta f) \sin (\Delta\alpha)$$

$$+ C_{L_W}(\alpha' - \Delta\alpha) \cos (\Delta\alpha)] \times .78 + \frac{1}{2} \rho S_W V^2 C_{L_W}(\alpha') \times .22$$

$$\alpha_R = \alpha - \Delta\alpha$$

$$\Delta\alpha = \arcsin [\frac{2\nu}{V_R} \sin (\phi)]$$

$$V_R^2 = V^2+4\nu^2+4V\nu \cos(\phi)$$

$$\alpha = \theta-\gamma+.085$$

$$\alpha' = \alpha+.409\ \delta f$$

$$\phi = \eta+\theta-\gamma$$

ν is a solution of

$$\nu[V^2+\nu^2+2V\nu \cos \phi]^{1/2} = \frac{T}{\rho \times S_R}$$

$$C_L(\alpha') = 4.28\ \alpha' \qquad \alpha_s'^- \leq \alpha' \leq \alpha'_s$$

$$= \frac{4.28\ \alpha_s'^+[\frac{\pi}{2} -.25\delta f+.409\delta f-\alpha']}{[\frac{\pi}{2} -.25\delta f+.409\delta f-\alpha_s'^+]} \qquad \alpha' > \alpha_s'^+$$

$$= \frac{4.28\ \alpha_s'^-[\frac{\pi}{2} + .25\delta f-.409\delta f+\alpha']}{[\frac{\pi}{2} +.25\delta f-.409\delta f+\alpha_s'^-]} \qquad \alpha' < \alpha_s'^-$$

$$C_D(\alpha',\delta f) = .025+.1\delta f^2+1.035\alpha'^2 \qquad \alpha_s'^- \leq \alpha' \leq \alpha_s'^+$$

$$= .025+.1\delta f^2+1.035\alpha_s'^{+2}+.62[\alpha'-\alpha_s'^+]$$

$$\alpha' > \alpha_s'^+$$

$$= .025+.1\delta f^2+1.035\alpha_s'^{-2}+.62(\alpha_s'^- -\alpha')$$

$$\alpha' < \alpha_s'^-$$

$$\alpha'^{+}_{s} = .317 + .205\delta f \text{ radians}$$

$$\alpha'^{-}_{s} = -.317 + .205\delta f \text{ radians}$$

$$D_T = \frac{1}{2} \rho V^2 S_T C_{D_T}(\alpha_T)$$

$$L_T = \frac{1}{2} \rho V^2 S_T D_{L_T}(\alpha_T)$$

$$C_{L_T}(\alpha_T) = 4.28\ \alpha_T \qquad |\alpha_T| \leq .317 \text{ rad}$$

$$= 1.08\ [\tfrac{\pi}{2} - \alpha_T] \qquad \alpha_T > .317 \text{ rad}$$

$$= -1.08\ [\tfrac{\pi}{2} + \alpha_T] \qquad \alpha_T < -.317 \text{ rad}$$

$$C_{D_T}(\alpha_T) = .025 + 1.035\alpha_T^2 \qquad |\alpha_T| \leq .307 \text{ rad}$$

$$= .1285 + .62(|\alpha_T| - .317) \qquad \alpha_T > .317 \text{ rad}$$

$$\alpha_T = \theta - \gamma - .01$$

$$D_F = \frac{1}{2} \rho V^2 S_F [.05 + .25 \sin^3(|\alpha_F|)]$$

$$L_F = \frac{1}{2} \rho V^2 S_F [.25 \sin^2(\alpha_F) \cos(\alpha_F)\ \mathrm{sgn}(\alpha_F)]$$

$$\alpha_F = \theta - \gamma$$

Nacelle lift and drag are neglected.

Thrust is determined as a function of the component of the free stream air speed perpendicular to rotor tip path plane. In the computer program linear interpolation is carried out between points spaced 15 m sec^{-1} apart

Normal Velocity	Max. Available Thrust
0 m sec^{-1}	211,000 N
15	153,500
30	118,500
45	92,500
60	71,800
75	57,000
90	47,500
105	40,750
120	36,250
135	33,000

Table B-1 Thrust as a Function of Free Stream Air Speed.

The longitudinal inplane rotor force is small under most flying conditions and is neglected.

m	mass of aircraft	= 12,700 Kg
mg	weight of aircraft	= 123,300 N
S_W	wing area	= 35.5 m^2
S_T	tail area	= 16.25 m^2
S_F	fuselage planform area	= 36.7 m^2
S_R	disc area of rotors (total)	= 216.3 m^2
ρ	density of air (at S_L)	= 1.267 kg m^{-3}

B.2 Linearized Equations

The nonlinear equations are linearized about the nominal path by numerical differentiation. They are

$$\frac{dZ}{dx} = F(x)Z + G(x)U$$

where

$$Z = \begin{bmatrix} \delta V \\ \delta \gamma \\ \delta h \\ w \end{bmatrix}$$

$$F = \begin{bmatrix} \frac{\partial f_1}{\partial V} & \frac{\partial f_1}{\partial \gamma} & 0 & \left(\frac{\partial f_1}{\partial V} + \frac{f_1}{V}\right)\cos\gamma - \frac{\sin\gamma}{V}\left(\frac{\partial f_1}{\partial \gamma} - f_1 \tan\gamma - V f_2\right) \\ \frac{\partial f_2}{\partial V} & \frac{\partial f_2}{\partial \gamma} & 0 & \left(\frac{\partial f_2}{\partial V} + \frac{2f_2}{V}\right)\cos\gamma = \frac{\sin\gamma}{V}\left(\frac{\partial f_2}{\partial \gamma} - f_2 \tan\gamma + \frac{f_1}{V}\right) \\ 0 & 0 & \sec^2\gamma & 0 \\ 0 & 0 & 0 & 0 \end{bmatrix}$$

for take-off

$$G(x) = \begin{bmatrix} \frac{\partial f_1}{\partial \eta} & \frac{\partial f_1}{\partial \theta} \\ \frac{\partial f_2}{\partial \eta} & \frac{\partial f_2}{\partial \theta} \\ 0 & 0 \\ 0 & 0 \end{bmatrix}, \quad U = \begin{bmatrix} \delta\eta \\ \delta\theta \end{bmatrix}$$

and for landing

$$G(x) = \begin{bmatrix} \frac{\partial f_1}{\partial \eta} & \frac{\partial f_1}{\partial T} \\ \frac{\partial f_2}{\partial \eta} & \frac{\partial f_2}{\partial T} \\ 0 & 0 \\ 0 & 0 \end{bmatrix}, \qquad U = \begin{bmatrix} \delta\eta \\ \delta T \end{bmatrix}$$

and

$$\frac{dV}{dx} = f_1$$

$$\frac{d\gamma}{dx} = f_2$$

B.3 Weighting Matrices

The following are the values of the weighting matrices used in the quadratic synthesis technique.

For take-off

$$A = \begin{bmatrix} .00021 & 0 & 0 & 0 \\ 0 & .04 & 0 & 0 \\ 0 & 0 & .00044\cos^2\gamma & 0 \\ 0 & 0 & 0 & 0 \end{bmatrix}$$

$$B^{-1} = \begin{bmatrix} .14V & 0 \\ 0 & \begin{cases} .3 & V > 24.5 \text{ m sec}^{-1} \\ 0 & V \leq 24.5 \text{ m sec}^{-1} \end{cases} \end{bmatrix}$$

$$S_f = \begin{bmatrix} .069 & 1.2 & .02 & -.0026 \\ 1.2 & 170 & 2.9 & 1.1 \\ .02 & 2.9 & .063 & .013 \\ -.0026 & 1.1 & .013 & .048 \end{bmatrix}$$

For landing:

$$A = \begin{bmatrix} .0011 & 0 & 0 & 0 \\ 0 & .04 & 0 & 0 \\ 0 & 0 & .00044 \cos^2\gamma & 0 \\ 0 & 0 & 0 & 0 \end{bmatrix}$$

$$B^{-1} = \begin{bmatrix} .082V & 0 \\ 0 & 2\times10^7 V \end{bmatrix}$$

and

$$S_{x_f} = \begin{bmatrix} .36 & .065 & -.0036 & -.04 \\ .065 & .032 & .0044 & -.06 \\ -.0036 & .0044 & .0072 & -.057 \\ -.04 & -.06 & -.057 & 240 \end{bmatrix}$$